Title

Alphavirus replicons encoding IFN-γ enhance cancer virotherapy by overcoming macrophage-mediated suppression

Authors and affiliations

Laura Horvathova[1]*, Priscilla Kinderman[2]*, Thijs Janzen[3], Baukje Nynke Hoogeboom[1], Franz J. Weissing[3], Nadine van Montfoort[2], Toos Daemen[1], Darshak K. Bhatt[1,4]

1. Department of Medical Microbiology and Infection Prevention, University Medical Center Groningen, University of Groningen, Groningen, The Netherlands
2. Department of Gastroenterology and Hepatology, Leiden University Medical Center, Leiden, The Netherlands
3. Groningen Institute for Evolutionary Life Sciences, University of Groningen, Groningen, The Netherlands
4. Lead contact: Darshak K. Bhatt (d.bhatt@umcg.nl)

* Equal contributions

Summary

Interference by tumor-associated macrophages may significantly reduce the efficacy of therapeutic viruses designed to infect cancer cells and activate antitumor T-cells. Using a computational model, we hypothesized that viruses encoding a T cell-stimulating signal, like IFN-γ, could overcome this barrier. We engineered an alphavirus-based replicon expressing IFN-γ and evaluated its effect in various human-derived tumor-immune coculture systems and an *in vivo* murine model. While alphavirus replicons do not replicate in macrophages, macrophages acted as a barrier, limiting tumor infection in a frequency-dependent but phenotype-independent manner. Nonetheless, T-cell activation occurred even when only a fraction of infected tumor cells expressed IFN-γ, regardless of macrophage presence, frequency, or phenotype. Additionally, viral stimulation drove macrophage-repolarization towards a pro-inflammatory phenotype favoring T-cell activation. These findings highlight a strategy for optimizing virotherapy in macrophage-rich tumors by designing viruses that stimulate T-cell activation, ensuring therapeutic efficacy.

Keywords

alphavirus replicons, tumor-associated macrophages, therapeutic resistance, computational model, tumor-immune coculture

Introduction

Tumor-associated macrophages are a predominant component of the tumor immune infiltrate across many cancers[1]. These macrophages exhibit context-dependent phenotypic plasticity[2,3] and function to either support or suppress antitumor immunity[2–5]. In particular, they perform phagocytosis, act as antigen-presenting cells, express checkpoint regulators, and secrete an array of cytokines that shape cancer progression and response to immunotherapy[4,6,7].

Cancer virotherapy is a form of immunotherapy where viruses are used to infect cancer cells, and subsequently boost anticancer T cell responses[8]. Virus-induced cancer cell death causes the release of danger signals and antigens in the tumor microenvironment[9]. Ideally, these signals are immunogenic, enhancing the recruitment and proinflammatory activation of immune cells into the tumor. However, tumor-associated macrophages may hinder the therapeutic efficacy of virotherapy by capturing virus particles, thereby significantly reducing the availability of the virus for infecting cancer cells[10–13]. This effect could be particularly pronounced when macrophages are non-permissive for viral replication, as it restricts tumor cell infection and the subsequent release of immunostimulatory signals and tumor antigens, thereby indirectly suppressing downstream anticancer T-cell activity. Tumor-associated macrophages further limit oncolysis through innate antiviral signaling[10–13] and T-cell suppression by regulatory mechanisms[3,14]. Variation in tumor composition[15,16], particularly in terms of macrophage frequency and phenotype can lead to variability in therapeutic responses[17–19]. Enhancing T-cell-mediated antitumor responses using virotherapy thus remains challenging, especially in macrophage-rich tumors. Therefore, development of therapeutic viruses capable of strongly stimulating T-cell immune responses is crucial to overcome the limitations posed by non-permissive macrophages.

Semliki Forest virus (SFV)-based replicons are emerging as promising candidates for immunogenic virotherapy. SFV is a positive-stranded RNA virus, belonging to the *Alphavirus* genus. The RNA genome of SFV functions as a replicon, encoding non-structural viral proteins capable of viral-RNA translation and replication. Previous efforts in developing recombinant SFV particles (rSFV) have focused on improving safety by deleting viral genes that code for structural proteins[20]. This creates suicidal virus particles capable of a single round of infection. We and others have demonstrated that rSFV particles can successfully infect and express viral genes in a wide range of cancer cells and healthy stromal cells, however, macrophages are non-permissive to SFV infections and virus-encoded protein translation[21–23]. Furthermore, the immunogenicity of rSFV has been improved by encoding antigens[24–27], cytokines[22,28], or antibodies[29] to boost humoral and cellular immune responses in the context of cancer therapy and vaccination against infectious diseases. Our group has demonstrated phase-1 and phase 2 clinical safety, immunogenic potential and clinical efficacy of an rSFV-based therapeutic vaccine encoding antigens of human papillomavirus in patients with cervical cancer[30,31]. So far, studies using rSFV as an anticancer agent have only been conducted in murine models[22,28,29]. Recently our group showed that rSFV can be engineered to express immunogenic human cytokines or chemokines with an enhanced potential to recruit and activate T-cells in different human cancer models[23].

In this study, we implemented a combined theoretical and experimental approach to design an immunogenic-rSFV therapy capable of T-cell activation and macrophage polarization. First, we evaluated whether indeed macrophages limit rSFV infection in cancer cells growing in monolayer (2D, two-dimensional) or spheroid-based (3D, three-dimensional) tumor-macrophage cocultures. Second, we employed a computational model to assess whether rSFV-encoding immunogenic signals can promote anticancer T-cell responses and tumor eradication despite the presence of macrophages. Third, we analyzed literature to identify interferon-gamma (IFN-γ) as a pro-

78 inflammatory cytokine capable of both macrophage and T-cell activation. We further evaluated the
79 correlation between intra-tumoral IFN-γ signature and activation of macrophages and T-cells using
80 data of cervical and pancreatic cancer patients available from The Cancer Genome Atlas (TCGA)[1]. For
81 experimental validation, we engineered rSFV to express IFN-γ upon infection of cancer cells and
82 employed both monolayer and spheroid-based tumor-immune cocultures to evaluate T-cell
83 activation. In these tumor-immune cocultures, we introduced macrophages of either a naïve (M_{naive})
84 or an IL-4-induced phenotype (M_{IL4}). Finally in a proof-of-concept study, we tested the efficacy of
85 rSFV in a pancreatic cancer mouse model. These models allowed us to assess how tumor infection
86 and T-cell activation are influenced by macrophages and to evaluate the immunogenic potential of
87 virus-encoded IFN-γ.

88

89 **Results**

90 *Effect of macrophage frequency and phenotype on rSFV-mediated tumor infection*

91 As a proof-of-concept, we performed all analyses in the context of two independent solid tumor
92 types, i.e. cervical and pancreatic cancer, with innate differences in immune signaling
93 (**Supplementary Figure 1**). rSFV-mediated infection of cancer cells leads to expression of encoded
94 transgenes but not production of progeny virus particles (as illustrated in **Figure 1A**). To validate our
95 findings in an experimental setup, we employed an *in vitro* cancer-macrophage coculture model in
96 either a monolayer or spheroid-based spatial organization (**Figure 1B**). This allowed us to have
97 control over factors such as the frequency and phenotype of macrophages and cancer cells. Using
98 real-time microscopy-based imaging, we studied the effect of macrophages in regulating rSFV
99 infection of a pancreatic cancer cell line (PANC-1). Figure 1C-D shows microscopy images resulting
100 from the spheroid (**Figure 1C**) or monolayer (**Figure 1D**) coculture setup consisting of cancer cells and
101 a varying frequency of macrophages. With an increasing frequency of macrophages (stained red in
102 the images) present in the coculture, we observed a decrease in virus infection (stained green,
103 expressing virus-encoded green fluorescent protein, GFP). We performed the cancer-macrophage
104 coculture in various setups, either varying only the frequency of macrophages (green bar) or the
105 frequencies of both macrophages and cancer cells (purple bar) (**Figure 1E**). In particular, we
106 confirmed[21,32] that virus-encoded GFP expression is restricted to cancer cells but not macrophages.
107 The decrease in the number of infected cells corresponds to a decrease in the absolute number of
108 target cancer cells and to a relative increase in the number of macrophages (**Figure 1F-G**), indicating
109 that presence of macrophages limits the effect of virotherapy.

110 We used non-polarized macrophages for the experiments presented in Figure 1. Since tumor-
111 associated macrophages can exhibit diverse phenotypic states, we specifically addressed the
112 contribution of two phenotypes most frequently found in the tumor microenvironment. For this, we
113 polarized them to either a classically activated anti-tumoral phenotype (M_{class} or M1-like) or an
114 alternatively activated pro-tumoral phenotype (M_{alter} or M2-like) through cytokine stimulation
115 (**Figure 2A**). Here, we used either a combination of LPS and IFN-γ to generate classically activated
116 macrophages ($M_{LPS+IFN\gamma}$), or IL-4 to generate alternatively activated macrophages (M_{IL4}). Pro-
117 inflammatory cell surface marker proteins such as CD80 and CD86 are upregulated in classically
118 activated $M_{LPS+IFN\gamma}$ macrophages, whereas regulatory markers like CD206 are more abundant in
119 alternatively activated M_{IL4} macrophages (**Figure 2B**) also corresponding to a distinct cellular state
120 (**Figure 2C**). We then assessed if the macrophage phenotype, in particular the alternatively activated
121 M_{IL4} phenotype that is most frequently found in tumors, influenced tumor infection by rSFV in
122 monolayer or spheroid cocultures (**Figure 2D-E**). We observed that the number of GFP+ cells reduced

with an increase in the number of macrophages, however, independent of the macrophage phenotype (**Figure 2F-G**), as there were no differences observed in the magnitude of reduction in GFP+ cancer cells between conditions that had either $M_{Naïve}$ or M_{IL4} polarized macrophages. This was also the case when macrophages were cocultured with a cervical cancer cell line (Ca-Ski) (**Figure 2H**).

Notably, cytokine-driven macrophage polarization had no impact on the expression of genes encoding SFV-entry receptors (**Supplementary Figure 2**). Furthermore, blocking JAK-STAT signaling to examine the role of type-I interferon in antiviral effects failed to improve rSFV infection in cancer cells (**Supplementary Figure 3**). Thus, the frequency of non-permissive macrophages, rather than antiviral signaling or their polarized phenotype, primarily contributed to the observed reduction in infection.

Model predictions regarding the effectiveness of immunogenic-rSFV therapy

In a previous study, we developed a spatiotemporal model to assess the effect of anticancer T-cell responses in response to immunogenic signals released upon virotherapy[33,34]. **Figure 3A** (left image) depicts a snapshot of a computer simulation with a tumor containing uninfected cancer cells, virus-infected cancer cells, and macrophages. Upon infection-caused cell death, the model assumes that virus-induced immunogenic signals are released in the neighborhood (as depicted in **Figure 3A** right and illustrated in **Figure 3B**) stimulating anticancer T-cell response. Using this model, we assessed the efficacy of rSFV encoding immunogenic signals as a non-replicating suicidal virotherapy. To estimate therapeutic success, we assessed the probability of tumor eradication caused by rSFV-infection and anticancer T-cell cytotoxicity. Panels **C** to **E** show, for five scenarios regarding the percentage of initially infected tumor cells (0-50%), how the probability of tumor eradication is related to the IFN-γ level produced per infected cell (**Figure 3C**), the degree of T-cell cytotoxicity (**Figure 3D**), and the frequency of macrophages at the time of rSFV therapy (**Figure 3E**). Generally, 30% initially infected cells are sufficient to promote tumor eradication even at low levels of immunogenic signal production. A minimum T-cell cytotoxicity level of 3 (corresponding to 3 target cells killed per cytotoxic T-cell per day) is required for an effective therapeutic outcome, as increasing numbers do not correspond with increased tumor eradication. Therapeutic outcome was found to be mainly determined by the percentage of initially infected cells producing immunogenic signals and not by the macrophage frequency. To guide the selection of effective immunogenic signals for rSFV-based therapy, we next consulted the literature to identify candidates with strong T-cell-activating potential.

The association between IFN-γ and macrophage-T-cell activation

We analyzed current literature to screen potential immunomodulatory cytokines produced and/or consumed by T-cells and macrophages. By re-evaluating previously published data[35], we found that IFN-γ produced by T-cells represents a unique antitumoral cytokine that has the potential to stimulate both macrophages and T-cells through JAK-STAT signaling pathway (**Figure 4A**) with an effective concentration ranging from 3 to 40 pM (**Figure 4B**).

Based on cervical and pancreatic cancer patient data from TCGA[1,36], we analyzed the correlation between the IFN-γ signature in tumor samples with the frequency of macrophages and T-cells and the phenotype of macrophages (**Figure 4C**). The IFN-γ signature applied here was derived from the TCGA pan-cancer immunogenomic analysis[1,36]. **Figure 4D** shows an overview of the correlation between the intratumoral IFN-γ signature and different phenotypes of macrophages and cytotoxic CD8 T-cells. The IFN-γ signature was found to positively correlate with a classically activated (M_{class} or M1-like) pro-inflammatory macrophage phenotype in both cervical (CESC) and pancreatic (PAAD) tumor samples (**Figure 4E, 4G**) but not with an alternatively activated (M_{alter} or M2-like)

168 immunosuppressive macrophage phenotype (**Figure 4F, 4H**). As T-cells are one of the primary cells
169 producing IFN-γ, we analyzed if there was a correlation between intra-tumoral CD8 T-cells and a
170 particular macrophage phenotype (**Figure 4I**). We observed a positive correlation between classically
171 activated (M_{class}) proinflammatory macrophages and the frequency of intra-tumoral CD8 T-cells
172 (**Figure 4J, 4L**). Inversely, there was a negative correlation between alternatively activated (M_{alter})
173 immunosuppressive macrophages and CD8 T-cell frequency (**Figure 4K, 4M**). These findings highlight
174 a link between IFN-γ–driven macrophage polarization and CD8 T-cell infiltration, prompting further
175 investigation into whether rSFV-delivered IFN-γ could enhance this interaction in tumor–immune
176 cocultures.

177 *T cell activation by rSFV in the presence of macrophages*

178 We treated monolayer cocultures of macrophages and cancer cells with rSFV and added peripheral
179 blood mononuclear cells (PBMCs) to the culture to introduce T-cells and evaluate their activation
180 (**Figure 5A**). Through flow cytometry, we quantified expression of immune activation (CD69) and
181 cytotoxic-degranulation (CD107a) markers as a proxy of CD4 (helper) and CD8 (cytotoxic) T-cell
182 activation. These markers were chosen from a broader panel of T-cell activation and regulation
183 markers (**Supplementary Figure 4,5**). T-cells were considered fully activated when simultaneously
184 positive for CD38, CD69, and CD107a expression. **Figure 5B and 5C** illustrate the population
185 distribution of activated CD4 and CD8 T-cells in different scenarios of rSFV infection and tumor-
186 immune cocultures consisting of either PANC-1 cells or Ca-Ski cells in culture with M_{naive} or M_{IL4}
187 macrophages in different frequencies. The upper right quadrant in each flow cytometry panel
188 indicates the population of fully activated T-cells as characterized by the expression of CD69 and
189 CD107a.

190 We observed a decrease in CD4 but not CD8 T-cell activation as a result of coculturing PBMCs solely
191 with either M_{naive} or M_{IL4} macrophages (black circle/line, **Figure 5D**, 6E leftmost panel). PBMC
192 coculture with cancer cells alone or in the presence of increasing frequency of either M_{naive} or M_{IL4}
193 macrophages also led to a similar decrease in CD4 T-cell activation when compared to PBMCs alone
194 (NT = no treatment, black circle/line, **Figure 5D**). rSFV particles themselves in the absence of target
195 cancer cells did not have any immunomodulatory effects on CD4 or CD8 T-cell activation directly
196 (green circle/line, **Figure 5D, 5E**, leftmost panel). Upon rSFV-GFP therapy, i.e. not encoding IFN-γ,
197 CD8 T-cell activation was only observed in the case of infecting Ca-Ski cells but not PANC-1 cells and
198 was independent of macrophage presence or phenotype (green circle/line, **Figure 5E**, rightmost
199 panel). Upon rSFV-IFN-γ (rSFV-encoding IFN-γ) treatment, however, both CD4 and CD8 T-cells were
200 activated independently of infecting Ca-Ski cells or PANC-1 cells (red circle/line, **Figure 5D, 5E**). Here,
201 CD4 T-cell activation increased with an increasing number of either M_{naive} or M_{IL4} macrophages
202 present in the coculture (**Figure 5D**). We confirmed that rSFV-encoded IFN-γ mediates T cell
203 activation by inhibiting JAK-STAT signaling in T cells. Treatment with ruxolitinib, in combination with
204 rSFV-IFN-γ, resulted in a reduced frequency of activated T cells as compared to when treated with
205 rSFV-IFN-γ alone (**Supplementary Figure 6**).

206 Next, we assessed T-cell activation in spheroid-based tumor-immune cocultures (**Figure 6A**). In
207 contrast to the results from the monolayer-based coculture system, we observed a decrease in the
208 number of activated CD4 T-cells with an increasing frequency of macrophages in the non-rSFV-
209 treated coculture (black circle/line, **Figure 6B**). However, similar to the results from the monolayer
210 coculture, we observed that rSFV-GFP particles only induced CD8 T-cell activation in the case of
211 infecting Ca-Ski cells but not PANC-1 cells (green circle/line, **Figure 6C**, rightmost panels). Moreover,
212 rSFV-IFN-γ also led to a higher frequency of activated CD4 and CD8 T-cells independent of whether it

213 infected Ca-Ski cells or PANC-1 cells (red circle/line, **Figure 6B, 6C**). Here, CD4 and CD8 T-cell
214 activation even improved further with an increasing frequency of either M_{naive} or M_{IL4} macrophages.

215 *Multimodal activation of macrophages by rSFV-IFN-γ*

216 Recently our group has shown that rSFV replicon virus particles have a direct influence on
217 macrophage phenotype and can lead to their pro-inflammatory activation, in part by JAK-STAT and
218 NF-κB signaling, independent of their initial state[32]. Consequently, we evaluated if macrophages are
219 also stimulated by infected cancer cells alone and if there is any additional effect in combination with
220 virus-mediated activation (**Figure 7A**). To quantify this response, we assessed the change in
221 expression of costimulatory molecules (CD80, CD86) on macrophages involved in T-cell regulation in
222 addition to CD206 expression that is often associated with a regulatory phenotype and poor cancer
223 prognosis. IL-4 polarized (M_{IL4}) regulatory macrophages were found to upregulate CD86 and CD80
224 cell-surface expression upon stimulation with either only rSFV particles (**Figure 7B**) or only PANC-1
225 infected cells expressing virus-encoded IFN-γ (**Figure 7C**) or both (**Figure 7D**). The upregulation of
226 CD80 and CD86 was the highest when macrophages received simultaneous stimulation by virus
227 particles and infected cells producing virus-encoded IFN-γ. Importantly, significant downregulation of
228 cell-surface CD206 expression was observed when macrophages were stimulated with infected cells
229 producing virus-encoded IFN-γ but not GFP. Notably, IL-4 polarized macrophages upregulated the T-
230 cell inhibitory ligand PD-L1 in the presence of cancer cells infected with rSFV-IFN-γ (**Supplementary**
231 **Figure 7**). This upregulation is likely driven by canonical IFN-γ signaling pathways. However it is
232 important to highlight that this phenomenon did not coincide with a reduction of T-cell activation
233 phenotype as shown in **Figure 5** and **6**.

234 We further confirmed that both naïve (M_{naive}) and regulatory (M_{IL4}) macrophages upregulate CD80
235 and CD86 cell-surface expression upon stimulation with rSFV replicon particles (**Figure 7F**).
236 Moreover, CD206 downregulation and a strong CD80 and CD86 upregulation were observed when
237 either of the macrophage types was stimulated simultaneously with rSFV particles and infected
238 cancer cells expressing virus-encoded IFN-γ (**Figure 7G-J**). This observation holds true for both PANC-
239 1 (panel **G-H**) and Ca-Ski (**panel I-J**) cancer cell lines.

240 Additionally, we confirmed that rSFV-encoded IFN-γ mediates macrophage activation through the
241 JAK-STAT pathway by evaluating macrophage phenotypes in the presence of the JAK inhibitor
242 ruxolitinib. We observed that rSFV-IFN-γ, but not rSFV-Flt3L (control stimuli for myeloid cell
243 activation) or rSFV-GFP mediated, infection of cancer cells led macrophage stimulation as measured
244 by increased expression of co-stimulatory, anti-tumoral markers (CD80, CD86) and reduced levels of
245 pro-tumoral markers (CD206). However, treatment with ruxolitinib attenuated these changes,
246 indicating that IFN-γ-driven macrophage activation is at least partially dependent on JAK-STAT
247 signaling (**Supplementary Figure 7**).

248 *Assessing the in vivo efficacy of rSFV-IFN-γ*

249 Finally in a proof-of-concept experiment, we studied the effect of intratumoral administration of
250 rSFV-IFN-γ on tumor growth and the tumor immune microenvironment (TME) in mice bearing
251 KPC3[56–58] pancreatic tumors (**Figure 8**). As demonstrated in (**Supplementary Figure 8**), these tumors
252 are rich in macrophages. When tumors were palpable, mice received three intratumoral injections of
253 PBS, rSFV-GFP, or rSFV-IFN-γ at doses of 10^7 or 10^8 particles on days 12, 13 and 14 post-tumor
254 implantation (illustrated in **Figure 8A)**, Seven days after the last injection, the immune cells in tumor
255 and spleen were analyzed by flow cytometry. Treatment with rSFV-IFN-γ at both doses markedly
256 showed a reduction in tumor size compared to PBS and rSFV-GFP, with the highest efficacy observed
257 at the 10^8 dose (**Figure 8B, Supplementary Figure 9**). Notably, the higher dose of rSFV-GFP (10^8) also

258 led to a measurable reduction in tumor size compared to PBS, indicating that replicon treatment
259 alone can elicit some degree of anti-tumor activity.

260 Flow cytometric analysis of tumors (**Figure 8C-N**) collected 7 days after the final injection revealed
261 enhanced infiltration of innate and adaptive immune cells in the rSFV-IFN-γ–treated groups.
262 Importantly, while total macrophage frequency **Figure 8C**) was not different between groups, a clear
263 shift in macrophage polarization was observed: pro-tumoral CD206^{+} macrophages were reduced
264 significantly (**Figure 8D, Supplementary Figure 9B**), and anti-tumoral MHCII^{+} macrophages were
265 enriched (**Figure 8E**) in the rSFV-IFN-γ–treated tumors. These changes were dose- and stimuli
266 dependent and most pronounced at the higher IFN-γ dose. Furthermore, increased frequencies of NK
267 cells, and CD8^{+} T-cell were found in the rSFV-IFN-γ groups compared to controls (**Figure 8F, I and L)**.
268 NK cells and CD8+ T cells expressed more markers associated with recent antigen exposure, including
269 CD69, CD44 and PD-1 across all rSFV-treated groups, compared to PBS-treated mice (**Figure 8 G, J, K,**
270 **N**).

271 Second, the systemic effects were analyzed in the spleen. This analysis revealed an increased depot
272 of CD3^{+} T-cells (Figure 8O) in mice treated specifically by the rSFV-IFN-γ virus, whereas general rSFV
273 treatment showed increased numbers of CD44+ CD4+ and CD8+ T-cell subsets (**Figure 8Q and 8R**).
274 These data indicate that intratumoral rSFV treatment not only modified the local immune subsets in
275 the TME, but also activated T-cells systemically.

276 Collectively, our data demonstrates that intratumoral administration of rSFV-IFN-γ can slow down
277 tumor growth and modulate the TME of immune-suppressive tumors towards a more immune-
278 infiltrated phenotype.

279

280 **Discussion**

281 In this study, we investigated how macrophages impact the therapeutic efficacy of rSFV-based
282 anticancer virotherapy. Our findings show that macrophages, regardless of their phenotype, do not
283 translate rSFV-encoded proteins[37] and simultaneously limit tumor cell infection. This highlights a
284 significant barrier to effective virotherapy, as the presence of macrophages can limit the subsequent
285 immunogenic activity of the virus, potentially reducing the overall therapeutic outcome[17,33]. Notably,
286 tumor-associated macrophages often adopt immunosuppressive phenotypes that support tumor
287 progression and contribute to an overall inhibitory tumor microenvironment. Leveraging a
288 computational modelling approach, we hypothesized that arming therapeutic viruses to express
289 immunogenic signals like IFN-γ could stimulate robust T-cell activation and re-polarize macrophages,
290 tipping the balance towards tumor eradication. This was experimentally validated in both *in vitro*
291 human-based tumor-immune cocultures and an *in vivo* murine tumor model. Overall, our results
292 demonstrate the potential of a combined theoretical and experimental approach in improving the
293 immunogenic potential of anticancer virotherapy.

294 Our computational modeling results provided insights into the spatiotemporal dynamics of rSFV-IFN-
295 γ therapy and its potential despite an abundant presence of macrophages. Our model demonstrated
296 that the predicted release of IFN-γ at effective concentrations is vital for achieving robust T-cell
297 activation and subsequent tumor eradication. Specifically, the model underscored the importance of
298 achieving the effective concentration threshold via either increasing the number of infected cells in
299 the tumor or by improving IFN-γ production by individual infected cells; in both cases ensuring
300 activation of anticancer cytotoxic T-cells to mount a strong antitumor response. The model also
301 highlighted the importance of T-cell cytotoxicity in the success of rSFV-IFN-γ therapy. A minimally

302 required cytotoxicity rate of three target cells killed per day by each cytotoxic T-cell, comparable to
303 what is noted in the literature[38], was found to be essential for effective tumor eradication. This
304 emphasizes that alongside the production of IFN-γ, the intrinsic killing efficiency of T-cells is a critical
305 factor in the overall therapeutic outcome. Importantly, the model predicted that the therapeutic
306 success is largely independent of the number of macrophages present at the time of treatment. This
307 suggests that rSFV-IFN-γ may effectively overcome the influence of macrophages non-permissive for
308 SFV, provided that the thresholds for infected cells and T-cell cytotoxicity are met.

309 These theoretical predictions were substantiated *in vivo* using the murine KPC3 pancreatic tumor
310 model, which is an aggressive, immunologically "cold" tumor[56–58] known for its dense macrophage-
311 rich barrier and poor T-cell infiltration. Intratumoral administration of rSFV-IFN-γ led to a marked
312 delay in tumor growth compared to controls. Flow cytometry analysis of tumor-infiltrating and
313 systemic immune cells confirmed an increased presence and activation of cytotoxic $CD8^+$ T-cells,
314 $CD4^+$ T-helper cells, NK cells, and a shift in macrophage phenotype from immunosuppressive to pro-
315 inflammatory populations. This immune reprogramming likely resulted from intra-tumoral IFN-γ
316 expression, macrophage repolarization, or both. Notably, while rSFV-IFN-γ was most effective, even
317 high-dose rSFV-GFP showed partial tumor growth delay, suggesting that viral infection and innate
318 immune stimulation alone contribute to therapeutic benefit. These findings collectively underscore
319 the potential of rSFV-IFN-γ virotherapy to enhance antitumor responses by leveraging the synergistic
320 effects of targeted viral infection and potent immune activation, regardless of the presence of
321 macrophages.

322 Based on our empirical findings, we confirm that rSFV while not infecting macrophages leads to their
323 immunogenic activation. Importantly, as the frequency of macrophages in coculture with cancer cells
324 increased, the infectivity of the cancer cells decreased in both monolayer and spheroid-based
325 settings. We confirmed that macrophages themselves did not allow rSFV-encoded transgene
326 expression, which can likely be attributed to innately active antiviral signaling pathways. This is in line
327 with our previous work[32] and the observations made by Olupe Kurena and colleagues[37]. Multiple
328 oncolytic viruses have been shown to activate macrophages during therapy, both through direct
329 virus-uptake and signaling from infected cancer cells[39–43]. Specifically for replication-competent
330 oncolytic viruses, macrophage activation has also been attributed to therapeutic resistance due to
331 virus-uptake by macrophages, antiviral signaling (e.g. via TNF-α or IFN pathway) and killing of
332 infected cancer cells to inhibit virus replication[42–44]. In case of replication-deficient virotherapy like
333 rSFV, previous studies have demonstrated that sensing of viral RNA by various endosomal toll-like
334 receptors (TLRs) and cytosolic retinoic acid-inducible gene I (RIG-I) receptor can result in degradation
335 of viral RNA to downregulate viral-protein expression in macrophages[9]. However, TLR and RIG-I
336 mediated sensing also may lead to the proinflammatory activation of macrophages[45,46]. In line with
337 our previous study[32], we observed that macrophages upregulate CD80 and CD86 surface protein
338 expression upon viral stimulation, corresponding to a stronger co-stimulatory signaling for antigen
339 presentation. This is attributed partially via activation of JAK-STAT and NF-κB signaling in
340 macrophages[32]. A similar macrophage activation profile was observed independent of their initial
341 naïve (M_{naive}) or regulatory (M_{IL4}) macrophage phenotype. Various groups have demonstrated so far
342 that although macrophages demonstrate functionally distinct phenotypes[47,48], they are capable of
343 switching through these phenotypes in response to environmental stimuli within 48 hours[49,50].
344 Despite their adaptability, macrophages maintain their non-permissive nature towards rSFV-
345 mediated transgene expression independent of their initial phenotype, their expression of rSFV-entry
346 receptors, and their switch towards a pro-inflammatory phenotype upon rSFV-mediated stimulation.

347 Engineering rSFV to encode IFN-γ in infected cancer cells enhanced macrophage polarization to a
348 proinflammatory phenotype, is consistent with the increased frequency of anti-tumoral macrophages
349 observed *in vivo* following rSFV-IFN-γ treatment. This aligns with previous findings where rSFV driven
350 IFN-γ expression induced a strong antitumor immune response and inhibited tumor growth in a
351 murine orthotopic breast cancer model, by promoting macrophage activation and remodeling the
352 tumor microenvironment[51]. In our study, macrophages upregulated pro-inflammatory markers
353 (CD80, CD86) and downregulated pro-tumoral markers (CD206) to a significantly higher magnitude
354 when in the presence of infected cancer cells expressing rSFV-encoded IFN-γ, as compared to being
355 stimulated by virus alone or rSFV-GFP and rSFV-Flt3L infected cancer cells, where Flt3L served as an
356 myeloid-stimulating control. We assume this to be a result of the bimodal stimulation by virus-
357 particles and extracellular sensing of IFN-γ. Previous studies have demonstrated that either type-I or
358 type-II IFNs are required for macrophages to polarize towards a strongly pro-inflammatory
359 phenotype when stimulated by stress signals like extracellular release of heat-shock proteins or
360 danger signal like bacterial lipopolysaccharides and viral RNA[48,49,52]. Therefore, it is likely that the
361 intracellular release of rSFV-RNA upon virus uptake in the macrophages and extracellular IFN-γ
362 produced by neighboring infected cancer cells results in their proinflammatory activation. We indeed
363 confirmed that macrophage activation by rSFV-encoded IFN-γ can be reversed upon blocking JAK-
364 STAT signaling. Furthermore, as we did not observe rSFV-mediated transgene expression by
365 macrophages, we consider that rSFV-encoded IFN-γ expression is limited to infected cancer cells and
366 that IFN-γ is not sensed in an autocrine manner by macrophages.

367 Our study demonstrates that rSFV-encoding IFN-γ significantly stimulates T-cell responses,
368 independent of the influence of macrophages. This was observed across both monolayer (2D) and
369 spheroid (3D) cocultures, as well as *in vivo* highlighting the robustness of this approach. In monolayer
370 cocultures, the presence of rSFV-IFN-γ led to pronounced activation of both CD4 and CD8 T-cells,
371 even in the presence of high macrophage frequencies. Here, T-cell activation relied on IFN-γ or
372 macrophage polarization and was diminished upon inhibition of JAK-STAT signaling. Notably,
373 macrophages, despite their non-permissiveness to SFV infection and potential for antiviral signaling,
374 did not impede T-cell activation induced by rSFV-IFN-γ. This finding underscores the potential of IFN-
375 γ as a powerful immunostimulatory cytokine that can override the suppressive effects of
376 macrophages in the tumor microenvironment. Furthermore, the impact of macrophage phenotype
377 and frequency on T-cell responses varied between monolayer and spheroid cocultures. In monolayer
378 systems, macrophages reduced CD4 but not CD8 T-cell activation, suggesting a differential regulatory
379 effect on helper versus cytotoxic T-cells. However, in spheroid cocultures, an increase in macrophage
380 frequency led to a reduction in activation of both CD4 and CD8 T-cells. Despite these variations, rSFV-
381 IFN-γ consistently promoted strong T-cell responses regardless of either a naïve (M_{naive}) or regulatory
382 (M_{IL4}) macrophage phenotype. Finally, in both monolayer and spheroid cocultures, a high frequency
383 of macrophages correlated to a stronger CD4 T-cell activation by rSFV-IFN-γ, which may be attributed
384 to rSFV-mediated proinflammatory activation of the macrophages. In addition to transgenic IFN-γ
385 expression, differences in innate cancer cell-mediated immune signaling were also found to influence
386 both macrophage and T-cell activation, as noted in a previous study[23]. Nevertheless, IFN-γ expression
387 in infected PANC-1 and Ca-Ski cells proved effective in inducing robust immune responses.
388 Observations of Meissner et al. corroborate our results, that encoding IFN-γ by a non-replicating
389 virotherapy, influenza A virus in their case, can promote tumor eradication through enhanced
390 immune responses and not primarily through virus-mediated oncolysis[53]. Indeed, a replication-
391 competent virotherapy causing extensive virus-mediated oncolysis in combination with IFN-γ
392 mediated immune stimulation can also lead to tumor eradication albeit with a risk of virus
393 persistence[54].

In conclusion, our study presents a compelling case for the use of rSFV-encoding IFN-γ as a means to enhance antitumor immune responses, effectively overcoming macrophage-mediated regulation of virus-infection and T-cell activation. The combination of computational modeling with experimental validation in diverse human tumor models, provides evidence supporting this therapeutic strategy. Future studies should explore the clinical translation of these findings, assessing the efficacy of rSFV-IFN-γ in preclinical models like patient-derived organoids to test its therapeutic potential in a patient-specific manner. The significant implications of our findings lie in their potential to inform the design of anticancer virotherapies, especially for tumors characterized by high macrophage infiltration and immune suppression.

Limitations of the study

The primary aim of our study was to assess and improve the efficacy of rSFV replicons in the context of tumor-associated macrophages in a human model. While our study demonstrates the potential of rSFV-encoding IFN-γ in enhancing T-cell immune responses, several limitations must be acknowledged. One significant limitation of our study is the lack of direct measurement of T-cell-mediated tumor cell killing *in vitro*, due to the unavailability of a tumor-specific T-cell model. However, the observed tumor growth inhibition and increased immune cell infiltration *in vivo* following rSFV-IFN-γ treatment provide indirect evidence supporting the functional relevance of the T-cell activation seen in our coculture systems. Furthermore, our study does not fully account for the complex interactions within the tumor immune microenvironment, focusing primarily on T-cell responses. This narrow focus may overlook the broader spectrum of immune cell dynamics and the potential contributions of other immune cells, such as dendritic cells. Additionally, the *in vitro* coculture models, while informative, do not fully replicate the *in vivo* human tumor microenvironment. Expanding the study to test different virotherapies in the context of *in vivo* humanized murine models with xenograft tumors or patient-derived organoids representing diverse tumor and HLA-types will be essential to validate these findings and to fully understand the therapeutic potential of immunogenic virotherapy in a clinical setting.

Acknowledgements

This study was partially funded by Stichting De Cock-Hadders (grant 2020-35) awarded to DB and by Stichting Overleven met alvleesklierkanker (grant SOAK 22.02) awarded to NvM. Part of the work has been performed at the UMCG Imaging and Microscopy Center (UMIC) and the Flow Cytometry Research Unit (FCU) which is sponsored by UMCG. We thank the Center for Information Technology of the University of Groningen for their support and for providing access to the Hábrók high-performance computing cluster. We acknowledge the Flow Cytometry Facility and animal facility at LUMC for their support with the *in vivo* study and immunological analyses.

Author contributions

All authors made substantial contributions to the manuscript.

LH: Writing and editing manuscript, Data collection and analysis, Validation, Visualization

PK: Writing and editing manuscript, Data collection and analysis, Validation, Visualization

TJ: Conceptualization, Writing and editing manuscript, Software, Data analysis, Visualization, Supervision

BNH: Writing and editing manuscript, Data collection and analysis, Validation, Visualization

436 **FJW:** Conceptualization, Writing and editing manuscript, Supervision

437 **NM**: Conceptualization, Writing and editing manuscript, Supervision, Funding acquisition

438 **TD:** Conceptualization, Writing and editing manuscript, Supervision, Funding acquisition

439 **DB:** Conceptualization, Writing and editing manuscript, Data collection and analysis, Software,
440 Visualization, Supervision, Funding acquisition

441

442

443 **Declaration of interests**

444 Toos Daemen is co-founder of ViciniVax, a spin-off from the University of Groningen, developing
445 therapeutic cancer vaccines.

446

447 **Figure titles and legends**

448 **Figure 1: Effect of macrophage frequency on rSFV-mediated tumor infection. (A)** Illustration
449 explaining the mode of action of rSFV encoding either GFP or an immunogenic signal used as a non-
450 replicating "suicidal" virotherapy. **(B)** Schematic of the experimental setup for studying rSFV infection
451 (MOI-10) in a pancreatic cancer cell line (PANC-1) cocultured with macrophages in both monolayer
452 (2D) and spheroid (3D) spatial organizations. The frequency of macrophages and cancer cells were
453 controlled at the time of initiating the coculture. The coculture setup showing representative images
454 of **(C)** spheroids or **(D)** monolayers composed of cancer cells, infected cells (green, GFP+ cells), and
455 varying frequencies of macrophages (red, stained with FarRed dye) after 24 hours post infection with
456 rSFV encoding GFP (rSFV-GFP). **(E)** Diagram illustrating experimental setups with varying frequencies
457 of macrophages and cancer cells. Top row (variable setup): Frequency of macrophages and cancer
458 cells are varied. Bottom row (constant setup): Frequency of macrophages is varied while cancer cells
459 are kept constant. The grey cells indicate empty space that can be occupied by either cancer cells or
460 macrophages. Quantitative analysis of GFP expression indicating virus infection in the **(F)** spheroid
461 and **(G)** monolayer coculture setups. The plots represent data from 4 replicates of respective
462 coculture methods. Data are presented as mean values ± SD.

463 **Figure 2: Effect of macrophage phenotype on rSFV-mediated tumor infection. (A)** Schematic of the
464 experimental setup for polarizing peripheral blood derived macrophages to either a naïve (M_{naive}) or
465 or an anti-tumoral ($M_{LPS+IFNγ}$ or M1-like), or a pro-tumoral (M_{IL4} or M2-like) phenotype using
466 cytokines. **(B)** The surface expression of immunomodulatory proteins involved in anti-tumoral (CD80,
467 CD86) and pro-tumoral (CD206, CD163) macrophage activity. **(C)** Principle component analysis of the
468 differences in the phenotypes of macrophages from various healthy blood donors (n=5).
469 Representative images of rSFV infection (green, GFP+ cells) in a pancreatic cancer cell line (PANC-1)
470 cocultured with M_{naive} and M_{IL4} macrophages in both spheroid **(D)** and monolayer **(E)** spatial
471 organizations. Quantitative analysis of GFP expression indicating virus infection (MOI-10) in the **(F)**
472 spheroid and **(G)** monolayer coculture of PANC-1 cells with M_{naive} and M_{IL4} macrophages. **(H)**
473 Quantification of GFP expression in monolayer coculture of Ca-Ski cancer cells with M_{naive} and M_{IL4}
474 macrophages. The plots represent data from 4 replicates of respective coculture methods. Data are
475 presented as mean values ± SD.

Figure 3: Predicting the outcomes of immunogenic-rSFV therapy using a spatiotemporal model of tumor development. (A) Snapshot of a simulation. Left: Spatial structure of a tumor containing uninfected cancer cells (red), virotherapy-infected cancer cells (green), and macrophages (blue). Right: Distribution of infection-induced immunogenic signals (magenta) released from dying infected cancer cells, which stimulate a cytotoxic anti-cancer T-cell response. **(B)** Time trajectory illustrating the dynamics of a suicidal rSFV-therapy. Initially, uninfected cancer cells are targeted by the virus and weakly attacked by T-cells. Over time, virus-killed cancer cells release immunogenic signals, boosting T-cell cytotoxicity. Finally, the boosting effect wanes as immunogenic signal-levels diminish. **(C)** Effect of the amount of immunogenic signal produced per infected cells on the probability of tumor eradication. The colors indicate five simulation scenarios differing in the percentage of infected cells at the time of infection. **(D)** The effect of anticancer T-cell cytotoxicity rates on the probability of tumor eradication. **(E)** The effect of macrophage frequency at the time of rSFV therapy on the probability of tumor eradication. When not specifically under consideration, the parameter values were kept at their default values: the amount of immunogenic signal released was set to 0.25, the T-cell cytotoxicity rate was set to 5, and the number of macrophages was set to 2500. Colored dotted lines indicate the mean values, colored envelopes indicate the 95% confidence interval obtained via bootstrapping. Each panel represents 10000 simulations for respective parameter combinations.

Figure 4: Impact of IFN-γ on tumor associated macrophage and T-cells in the tumor microenvironment. (A) Schematic of cytokine production and reception by T-cells and macrophages (MØ), highlighting IFN-γ, IL-10, and IL-4 as key cytokines involved in influencing both cell types. Cytokine interactions are color-coded based on their impact on tumor progression: pro-tumoral (purple) and antitumoral (orange). **(B)** The effective concentration range of various cytokines (EC_{50}) with the points indicating the maximum and minimum experimentally reported limits (as per [35]). **(C)** Analysis process of cervical (CESC, 300 samples) and pancreatic (PAAD, 151 samples) cancer patient datasets stored at The Cancer Genome Atlas (TCGA) by using the CRI iAtlas online platform to correlate the presence of macrophage types with T-cells and IFN-γ signature. **(D)** Correlation heatmap of intra-tumoral IFN-γ signature with presence of various macrophage phenotypes. **(E-H)** Scatter plots showing the relationship between the intra-tumoral IFN-γ signature with the presence of classical (M_{class} or M1-like) and alternatively activated (M_{alter} or M2-like) macrophages in cervical or pancreatic cancer patients. **(I)** Correlation heatmap of intra-tumoral fraction of cytotoxic (CD8) T-cells with presence of various macrophage phenotypes. **(J-M)** Scatter plots showing the relationship between the intra-tumoral fraction of CD8 T-cells with the presence of M_{class} or M_{alter} macrophages in cervical or pancreatic cancer patients. In E-F and J-M, bivariate linear regression was performed to assess correlation, with r (correlation coefficient) and p-values indicated per plot.

Figure 5: Evaluation of T-cell activation in tumor-immune monolayer cocultures by rSFV. (A) Schematic representation of the experimental setup consisting of tumor-immune monolayer cocultures of cancer cells and macrophages treated with rSFV (MOI-10), followed by the addition of PBMCs to introduce T-cells and evaluate their activation. Flow cytometry analysis to measure activation of **(B)** CD4 helper T-cells and **(C)** CD8 cytotoxic T-cells based on the expression of CD69 and CD107a proteins, marked in the upper right quadrant in each panel. rSFV-GFP treated cocultures are indicated in green, rSFV-IFN-γ treated cocultures in red and non-infected (NT) in black. The representative plots in (B-C) illustrate T-cell activation in the context of PANC-1 cancer cells in coculture with either M_{naive} or M_{IL4} macrophages in different frequencies. Quantification of **(D)** CD4 helper T-cell or **(E)** CD8 cytotoxic T-cell activation in the tumor-immune cocultures by rSFV. The plots represent data from 4 replicates. Data are presented as mean values ± SD.

Figure 6: Evaluation of T-cell activation in tumor-immune spheroid co-cultures upon rSFV infection. (A) Schematic representation of the experimental setup consisting of tumor-immune spheroid cocultures of cancer cells and macrophages treated with rSFV, followed by the addition of PBMCs to introduce T-cells and evaluate their activation. Flow cytometry analysis to measure activation of T-cells as explained in Figure 6. Quantification of **(B)** CD4 helper T-cell or **(C)** CD8 cytotoxic T-cell activation in the tumor-immune cocultures by rSFV. rSFV-GFP treated cocultures are indicated in green and rSFV-IFN-γ treated cocultures in red. The plots represent data from 4 replicates. Data are presented as mean values ± SD.

Figure 7: Influence of rSFV infection on macrophage phenotype. (A) Experimental setup to study changes in macrophage phenotype upon stimulation by rSFV (MOI-10). This includes studying the effect of **(B)** either rSFV-particles alone (rSFV row), **(C)** or by infected cells alone, **(D)** or by both. **(E)** Heatmap of change in cell-surface expression of proteins involved in either pro-tumoral (CD206) or anti-tumoral (CD80, CD86) function of M_{IL4} macrophages cocultured or not with PANC-1 cancer cells upon stimulation resulting from rSFV particles and/or infected cells. Heatmap of M_{naive} and M_{IL4} macrophage cell-surface protein expression upon stimulation with **(F)** rSFV particles alone (bottom two rows), or both virus particles and infected **(G-H)** PANC-1 or **(I-J)** Ca-Ski cancer cells. The plots represent mean value data from 4 replicates.

Figure 8: Intratumoral virotherapy with rSFV-IFN-γ induces anti-tumoral macrophage polarization and immune cell infiltration in KPC3 tumor-bearing mice. (A) C57BL/6 mice were subcutaneously injected with KPC3 tumor cells (2×10^5) on day 0, and received intra-tumoral virotherapy with PBS (untreated control) or rSFV-replicons encoding either GFP or IFN-γ at doses of 10^7 or 10^8 particles per injection on days 12, 13 and 14. (B) Individual tumor growth across treatment groups, with untreated (black filled circles), SFV-GFP 10^7 (green empty circles), SFV-GFP 10^8 (green filled circles), SFV-IFN-γ 10^7 (red empty circles), and SFV-IFN-γ 10^8 (red filled circles). (C–N) Flow cytometric analysis of percentage tumor-infiltrating immune cells 7 days post-treatment: (C) total F4/80+ macrophages, (D) pro-tumoral $CD206^+$ macrophages, (E) anti-tumoral MHCII+ macrophages, (F) NK cells, (G) $CD69^+$ NK cells, (H) $KLRG1^+$ NK cells, (I) $CD8^+$ T cells, (J) $CD44^+$ $CD8^+$ T cells, (K) $PD\text{-}1^+$ $CD8^+$ T cells, (L) $CD4^+$ T cells, (M) $CD44^+$ $CD4^+$ T cells, (N) $PD\text{-}1^+$ $CD4^+$ T cells. (O–R) Flow cytometric analysis of splenic immune cells: (O) $CD3^+$ T cells, (P) $CD69^+$ NK cells, (Q) $CD44^+$ $CD8^+$ T cells, (R) $CD44^+$ $CD4^+$ T cells. Each symbol represents an individual mouse (n=6–7 per group), with bars indicating mean ± SEM. To evaluate differences in tumor growth and immune cell infiltration following virotherapy across treatment groups, data were analyzed using one-way ANOVA to assess statistical significance, with p-value indicated per comparison. The individual tumor growth curves for respective groups are shown in **supplementary figure 9** and the flow cytometry gating strategy is illustrated in **supplementary figure 10**.

STAR Methods

Key resources table

REAGENT or RESOURCE	SOURCE	IDENTIFIER
Antibodies		
anti-human CD4 (OKT4) FITC	Biolegend	317408
anti-human CD8 (SK11) APC-Cy7	Biolegend	344714
anti-human CD38 (HIT2) BV421	Biolegend	303526
anti-human CD69 (FN50) APC	Biolegend	310910

anti-human CD107a (H4A3) PE	Biolegend	328608
anti-human CD223 (LAG-3) (11C3C65) PE	Biolegend	369306
anti-human CD152 (CTLA-4) (BNI3) BV421	Biolegend	369606
anti-human CD279 (PD-1) (A17188B) APC	Biolegend	621610
anti-human CD11b (ICRF44) PE	Biolegend	301306
anti-human CD206 (15-2) APC-Fire	Biolegend	321133
anti-human CD80 (2D10) APC	Biolegend	374204
anti-human CD86 (BU63) FITC	Biolegend	328608
anti-human CD163 (GHI/61) PE	Biolegend	333605
anti-human CD68 (Y1/82A) PE-Cy7	Biolegend	333815
anti-human CD206 (MMR) APC	Biolegend	321109
anti-human CD80 (2D10) BV421	Biolegend	305221
anti-murine CD45.2 (104) FITC	Biolegend	109806
anti murine CD45.2 (104) AF700	Biolegend	109822
anti-murine CD3 (145-2C11) PE-CF594	BD Biosciences	562286
anti-murine CD8α (53-6.7) AF700	eBioscience	56-0081-82
anti-murine NK1.1 (PK136) BV650	BD Biosciences	564143
anti-murine CD4 (RM4-5) APC	BioLegend	100547
anti-murine F4/80 (BM8) PE-Cy7	Biolegend	123114
anti-murine CD206 (C068C2) BV711	Biolegend	141727
anti-murine Ly6G (1A8) BV786	Biolegend	127645
anti murine Ly6C (HK1.4) BV605	Biolegend	128036
Anti mouse/human CD44 (IM7) BV785	Biolegend	103059
Anti mouse CD69 (H1.2F4) FITC	eBioscience	11-0691-82
Anti mouse KLRG1 PE-Cy7	eBioscience	25-5893-82
Anti mouse CD279 (PD-1) (28F.1A12) PE	Biolegend	135205
anti-murine MHC-II (M5/114) BV421	BD Biosciences	562564
Zombie aqua viability dye	Biolegend	423102
Bacterial and virus strains		
Plasmid (Helper-2 and SFV-transgene) constructs to produce recombinant SFV replicon particles	Liljestrom lab, Karolinska Institutet Sweden	NA
E coli K12 JM110	Agilent	200239
rSFV-GFP	This study (in-house)	NA
rSFV-IFN-γ	This study (in-house)	NA
Biological samples		
Human buffy coats for PBMC isolation from HLA-A*02:01-typed healthy donors	Sanquin, Nijmegen, The Netherlands	NA
Chemicals, peptides, and recombinant proteins		
Restriction enzyme PspOMI Restriction enzyme XmaI	ThermoFischer Scientific ThermoFischer Scientific	ER0131 ER0171
Restriction enzyme SpeI	ThermoFischer Scientific	ER1251
SP6 polymerase	Amersham Pharmacia Biotech, Piscataway, US	NA

Celltrace FarRed dye	Invitrogen	C34572
Ruxolitinib	Stem Cell Technologies	73402
α-chymotrypsin	Sigma Aldrich	C4129
Aprotinin	Sigma Aldrich	A1153
Macrophage colony stimulating factor (M-CSF)	Biolegend	572903
Interleukin-4 (IL-4)	Biolegend	574004
Interferon-gamma (IFN-γ)	Biolegend	570204
Lipopolysaccharides (LPS) from *E. coli* O128:B12	Sigma Aldrich	L2755
LIberase TL	Sigma Aldrich	05401020001
Mouse BD Fc block (anti-mouse CD16 and CD32)	BD Biosciences	553142
Hydrogen peroxidase ELK powder	VWR Campina	7422478 NA
Rat, anti-mouse F4/80 antibody	Sanbio	CI:A3-1
Biotinylated rabbit anti-rat antibody	Agilent	NA
VECTASTAIN Elite ABC HRP Kit	Vector laboratories	PK-6100
Entellan	Sigma Aldrich	107960
Critical commercial assays		
NA		
Deposited data		
NA		
Experimental models: Cell lines		
Hamster, BHK-21 cells	ATCC	ccl-10
Human, PANC-1 cells	ATCC	crl-1469
Human, Ca-Ski	ATCC	crl-1550
Murine, KPC3 cells	Nadine van Montfoort lab, Leiden University Medical Center, Leiden	RRID:CVCL_A9ZK
Experimental models: Organisms/strains		
C57BL/6J mice	Charles River Laboratories	C57BL/6NCrl
Oligonucleotides		
NA		
Recombinant DNA		
Human IFN-gamma gene	This paper	NA
Murine IFN-gamma gene	This paper	NA
Software and algorithms		
Graphpad Prism	Graphpad	https://www.graphpad.com/
Incucyte® Software Modules	Sartorious	https://www.sartorius.com/
Qpath FlowJo	Qpath FlowJo	https://qupath.github.io/ https://www.flowjo.com/
Rstudio	Posit (Rstudio)	http://www.posit.co/

RawGraphs	RawGraphs	https://www.rawgraphs.io/
Other		
Nunclon Sphera 96 well plates	ThermoFischer Scientific	174925
Oncolytic Virus Immune simulator (OVI) model	This paper	https://github.com/rugtres/OVI/tree/macrophage
Superfrost Plus slides	VWR	48311-703

559

560 **Resource availability**

561 Lead contact: Further information and requests for resources and reagents should be directed to and
562 will be fulfilled by the lead contact Darshak K. Bhatt (d.bhatt@umcg.nl)

563 Material availability: All unique/stable reagents generated in the study are available upon request,
564 except where restricted by institutional agreements or MTAs.

565 Data and code availability:

566 - All data reported in this paper will be shared by the lead contact upon request.
567 - Any additional information required to reanalyze the data reported in this paper is available
568 from the lead contact upon request.
569 - The code used for this work and an executable version of the Oncolytic Virus Immune
570 simulator (OVI) can be found at https://github.com/rugtres/OVI/tree/macrophage.

571

572 **Method details**

573 TCGA analysis: We used the online CRI iAtlas portal to analyze TCGA data of cervical and pancreatic
574 cancer patients[1,36]. We selected the TCGA cohort of cervical cancer (CESC) patients (n=300) and
575 pancreatic cancer (PAAD) patients (n=151). Performed Pearson correlation to analyze the
576 relationship between IFN-γ signature, cytotoxic CD8 T-cells, and pro-tumoral (M2-like or M_{alter}) or
577 anti-tumoral (M1-like or M_{class}) macrophages. IFN-γ signature and immune cell subset quantifications
578 of the tumor samples were performed previously as a part of the immune landscape analysis of
579 cancer[1,36].

580 Computational model: In our previous work[33,34], we developed a spatiotemporal model for the effect
581 of anticancer virotherapy on tumor development to evaluate how anticancer T-cell responses
582 triggered by immunogenic signals affect the therapeutic outcome. In the current study, we employed
583 the model to simulate a tumor environment with three cell types: stromal macrophages, uninfected
584 infection-sensitive cancer cells, and infected cancer cells. We assumed that infection-sensitive cancer
585 cells and stromal macrophages are initially distributed randomly. Cells can divide, change status, or
586 die, with varying rates across cell types. Cancer cells can be infected by a therapeutic virus, which
587 targets and kills them, while stromal macrophages are non-permissive to infection. Since rSFV is a
588 non-replicating virotherapy, no further viral spread occurs in the model. We incorporated a cell-
589 specific immune response to assess how virus-induced immunogenic signals influence therapeutic
590 outcomes. The model assumes that infection-induced cell death induces the release of immunogenic
591 signals, which diffuses and subsequently activates T-cells to kill cancer cells, with cytotoxicity of the
592 activated T-cells depending on the local concentration of immunogenic signals. Key variables
593 assessed in this study include the percentage of infected cancer cells, amount of immunogenic signal
594 released per infected cell, T-cell cytotoxicity rate, and macrophage frequency. Immunogenic
595 molecules are initially absent and increase in concentration (λ) in the grid cell upon infection-induced
596 cell death. Immunogenic signals disperse to neighboring cells via diffusion and diminishes over time
597 due to evaporation. In our previous studies, the model revealed that therapeutic outcomes are
598 probabilistic. To account for this, we ran 10,000 simulations per parameter combination to capture
599 stochastic variations in the results. Since rSFV is a suicidal virotherapy and does not replicate, the
600 model predicted two possible outcomes at 1,000 days: (i) total tumor eradication, where all cancer
601 cells are eliminated; or (ii) tumor persistence, where cancer cells survive due to insufficient virus-
602 and/or immune-mediated killing. For this study, we focused on the probability of total tumor

603 eradication as the primary outcome. A detailed description of the model can be found in references
604 33 and 34. The code used for this work and an executable version of the Oncolytic Virus Immune
605 simulator (OVI) can be found at https://github.com/rugtres/OVI/tree/macrophage.

606 Cell culture: BHK-21, Ca-Ski, and Panc-1 cells were cultured in RPMI 1640 medium supplemented
607 with 10% fetal bovine serum (FBS), 100 U/ml penicillin, and 100 µg/ml streptomycin (P/S, Thermo
608 Scientific). Since, PANC-1 and Ca-Ski cells are HLA-A*02:01-restricted, we performed the cancer-
609 immune coculture assays with peripheral blood mononuclear cells (PBMCs) derived from HLA-
610 A*02:01-matched healthy donors (Sanquin, Netherlands). Cancer cell-macrophage cocultures were
611 cultured in RPMI 1640 medium supplemented with 10% FBS and 100 U/ml penicillin, 100 µg/ml
612 streptomycin. Cocultures with PBMCs were similarly cultured in RPMI 1640 medium supplemented
613 with 10% FBS and 100 U/ml penicillin, 100 µg/ml streptomycin. For spheroid cocultures, cells were
614 seeded in NuncSphera round-bottom 96-well plates (Thermo Fischer) and centrifuged for 10 minutes
615 at 1500 RPM. All cells were maintained in an incubator at 37°C with 5% CO_2.

616 Monocyte derived macrophage differentiation and polarization: Peripheral blood derived monocytes
617 were differentiated to macrophages and polarized in RPMI 1640 medium supplemented with 10%
618 FBS, 100 U/ml penicillin, 100 µg/ml streptomycin, 1mM sodium pyruvate (Thermo Scientific), non-
619 essential amino-acids (NEAA, Thermo Fisher), and 100 ng/mL macrophage colony-stimulating factor
620 (M-CSF, BioLegend San Diego, CA, USA). Briefly, PBMCs from healthy donors were cultured for 2
621 hours to allow monocyte adherence. Afterward, non-adherent cells were gently removed. The
622 adhered cells were stimulated with medium containing 100 ng/ml M-CSF. The medium containing M-
623 CSF was refreshed on 3 days post culture. Macrophages were replated on 7 days of culture. 24 hours
624 later, macrophages were polarized to either a M_{IL4} state with medium containing 20 ng/mL IL-4
625 (BioLegend, San Diego, CA, USA), or a M1-like state with medium containing 20 ng/ml IFN-γ and 100
626 ng/ml lipopolysaccharides (LPS), or were kept unstimulated (M_{naive}).

627 Design, production and titer determination of rSFV: We have previously designed rSFV-replicon
628 particles expressing immunogenic transgenes and capable of a single round of infection[23,55]. Briefly,
629 enhanced green fluorescent protein (GFP) and IFN-γ (human and murine versions) as transgenes
630 were ordered as a DNA construct (Eurofins Genomics, Ebensburg, Germany) and were cloned in the
631 SFV-replicon backbone plasmid (pSFV) by using PspOMI and XmaI as restriction sites and *E. coli*
632 JM110 as the competent cell chassis. Sanger sequencing was performed on isolated clones to
633 validate insertion (Eurofins Genomics). pSFV containing either GFP or IFN-γ and a SFV-Helper-2
634 plasmid (hSFV) were linearized with SpeI digestion (Life Technologies) for *in vitro* RNA synthesis by
635 SP6 polymerase reaction (Amersham Pharmacia Biotech, Piscataway, US). Next, pSFV-transgene RNA
636 and hSFV RNA were mixed in a 2:1 ratio and co-transfected in BHK21 cells in the presence of
637 electroporation buffer using the BioRad Gene Pulser II system (2 pulses, 850 V/25 µF; Biorad,
638 Hercules, U.S.A.). After electroporation, the cells were cultured in RPMI 1640 media supplemented
639 with 5% FBS, 100 U/ml penicillin, and 100 µg/ml streptomycin for 48 hours at 30°C with 5% CO_2. The
640 rSFV-transgene particles were purified by discontinuous sucrose density gradient ultracentrifugation
641 and stored in TNE buffer as aliquots at -80°C. Before use, all rSFV particles were activated by the
642 addition of 1:20 volume 10 mg/ml α-chymotrypsin (Sigma Chemical, St. Louis, US) and 2 mM $CaCl_2$ for
643 30 minutes to cleave the mutated spike proteins. After which, the α-chymotrypsin was inactivated by
644 the addition of 1:2 volume 2 mg/ml aprotinin (Sigma Chemical). Finally, the titer determination of
645 rSFV-particles was performed as described previously. Briefly, rSFV-particles were titrated by serial
646 dilution on monolayers of BHK-21 cells cultured in LabTek slides. After infection and incubation for 24
647 hours, the cells were fixed in 10% (w/v) acetone and further stained for nsP3 using a primary
648 polyclonal rabbit-anti-nsP3 antibody (1:2000 dilution), whilst a secondary Cy3-labeled animal-anti-

649 rabbit antibody (1:200 dilution) was used to amplify the signal. Positive cells were counted using
650 fluorescence microscopy, and the titers were determined.

651 Evaluating virus-infection in macrophage-cancer cell cocultures: M_{naive} or M_{IL4} macrophages were
652 differentiated from human PBMCs as described above. Different frequencies of M0 or M_{IL4}
653 macrophages were cocultured with either a constant or variable frequency of Panc-1 or Ca-Ski cancer
654 cells. When specified, macrophages were stained with CellTrace™ Far Red dye (ThermoFischer
655 Scientific, C34564) following the recommended protocol from the manufacturer. After overnight
656 incubation, cocultures were infected with an MOI of 10 (multiplicity-of-infection) of rSFV-GFP. The
657 ability of rSFV-particles to infect cells and express GFP was monitored over 24 hours by Incucyte-
658 based brightfield and fluorescence microscopy. The number of GFP-positive cells served as a measure
659 of the rSFV-GFP particle's infectivity.

660 Evaluating macrophage activation by virus particles and infected cancer cells: M_{naive} or M_{IL4}
661 macrophages were differentiated from human PBMCs as described above. M_{naive} or M_{IL4}
662 macrophages were cocultured in a 1:2 ratio with Panc-1 or Ca-Ski cells in a 24-well plate. After
663 overnight incubation, cocultures were infected with MOI-10 of rSFV-GFP or rSFV-IFN-γ. 24 hours
664 post-infection (HPI), all cells were collected and processed for Flow cytometry-based analysis of
665 macrophage activation markers. The gating strategy is illustrated in **Supplementary Figure 7**.

666 Evaluating T-cell activation in tumor-immune cocultures: M_{naive} or M_{IL4} macrophages were
667 differentiated as described above, from HLA-A*02:01 typed healthy donors. They were cocultured
668 with Panc-1 cells or Ca-Ski cells for 24 hours in 2 tumor cells to 1 macrophage cell ratio (15 000 cells
669 per well) in a treated 96-well plate. Cocultures were then infected with MOI-10 of rSFV-particles
670 encoding GFP or IFN-γ. 8 hours post-infection, freshly thawed PBMCs (from the same donor as used
671 for generating macrophages) were added to the cocultures (75 000 cells per well). 18 hours post
672 PBMCs addition, all cells were collected and stained for CD4 and CD8 T-cell population, as well as
673 immune activation cell surface markers, and analyzed *via* Flow cytometry. The gating strategy is
674 illustrated in **Supplementary Figure 4**.

675 Animal experiments: *In vivo* experiments were conducted as described previously[56–58]. In brief, male
676 C57BL/6J mice (6–8 weeks old; were obtained from Charles River Laboratories and housed in
677 individually ventilated cages (3-4 mice/cage) at the LUMC animal facility. The experiment was
678 reviewed, ethically approved, and registered by the institutional Animal Welfare Body of Leiden
679 University Medical Center. The experiment was carried out in compliance with Dutch and EU
680 regulations on animal experimentation under project license AVD1160020187004, issued by the
681 competent authority on animal experiments in the Netherlands. After one week of acclimatization,
682 mice were subcutaneously injected in the right flank with 2×10^5 KPC3 cells in 100 µL PBS/0.1% BSA.
683 Once tumors became palpable, mice were stratified into groups with similar average tumor volumes
684 and treated intratumorally under isoflurane anesthesia with 10^7 or 10^8 infectious particles of rSFV-
685 GFP, rSFV-IFN-γ, or PBS (30 µL) on three consecutive days. In contrast to the previous experiments,
686 rSFV-encoding murine-IFN-γ was used. Tumor volume, welfare and body weight were monitored
687 thrice weekly using calipers (tumor volume = length × width × height), blinded when possible. Mice
688 were sacrificed for immune profiling 7 days post-treatment or earlier if they reached human
689 endpoint, as described to be tumors exceeding 1000mm^3, signs of tumor ulceration or non-
690 experimental related complications (n=1 mouse, that was excluded due to fighting wounds). Tumors
691 were digested with Liberase TL for 15 min at 37°C, and processed into single-cell suspensions. Cells
692 were stained with Zombie Aqua viability dye, incubated with Mouse BD Fc Block™ (anti-Mouse
693 CD16/CD32), stained for cell surface markers and fixed in 1% paraformaldehyde. Flow cytometry was

694 performed on a BD LSRFortessa X20 at the LUMC Flow Cytometry Facility and analyzed using FlowJo
695 v10. The gating strategy is illustrated in **Supplementary Figure 10**.

696 Immunohistochemistry staining: Formalin fixed tumors were embedded in paraffin and sectioned at
697 4µm before placing on Superfrost® Plus slides (VWR). Sections were dried overnight at 37°C and
698 stored at 4°C until staining. Slides were deparaffinized and endogenous peroxidase was blocked with
699 0,3% hydrogen peroxidase (VWR) in methanol for 20 minutes. Rehydration was followed by 16
700 minute boiling in Trypsin/Calcium chloride solution (pH 7,4) followed by blocking with 0,2% ELK
701 (Campina) in PBS/0,1% BSA. Overnight incubation with primary rat anti-mouse F4/80 (Cl:A3-1,
702 Sanbio) was performed at RT in humidified box. The next morning, samples were incubated for 30
703 minutes at RT with biotinylated rabbit anti-rat (Agilent), followed by 30 minutes incubation with
704 avidin-biotin complex (VECTASTAIN® Elite® ABC HRP Kit; Vector Laboratories). Peroxidase activity was
705 detected using the 2-component liquid DAB+ system (Agilent) according to the manufacturer's
706 instructions for 5 min. Counterstaining was performed using hematoxylin (Sigma Aldrich) for 15
707 seconds, followed by dehydration and mounting using Entellan (Sigma Aldrich). Slides were scanned
708 using Zeiss Axio Scan Z.1 and processed with QuPath.

709 **Quantification and statistical analysis:** Experimental data represents the mean ± SEM of the number
710 of replicates. Statistical analysis of the data is specified in the respective figure legends when
711 applicable. For linear correlation, bivariate linear regression was performed, with r (correlation
712 coefficient) and p-values indicated per plot. one-way ANOVA was also used to compare groups and
713 assess statistical significance, with p-value indicated in the plots per comparison. Graphs were made
714 using Rstudio, RawGraphs, and Graphpad Prism 10.

715

716 **Supplementary file**

717 All the supplementary figures can be found in the supplementary document.

718 **References**

719 1. Thorsson, V., Gibbs, D.L., Brown, S.D., Wolf, D., Bortone, D.S., Ou Yang, T.-H., Porta-Pardo, E.,
720 Gao, G.F., Plaisier, C.L., Eddy, J.A., et al. (2018). The Immune Landscape of Cancer. Immunity *48*,
721 812-830.e14. https://doi.org/10.1016/j.immuni.2018.03.023.

722 2. Park, M.D., Silvin, A., Ginhoux, F., and Merad, M. (2022). Macrophages in health and disease. Cell
723 *185*, 4259–4279. https://doi.org/10.1016/j.cell.2022.10.007.

724 3. Biswas, S.K., and Mantovani, A. (2010). Macrophage plasticity and interaction with lymphocyte
725 subsets: cancer as a paradigm. Nat Immunol *11*, 889–896. https://doi.org/10.1038/ni.1937.

726 4. Fridman, W.H., Zitvogel, L., Sautès–Fridman, C., and Kroemer, G. (2017). The immune contexture
727 in cancer prognosis and treatment. Nat Rev Clin Oncol *14*, 717–734.
728 https://doi.org/10.1038/nrclinonc.2017.101.

729 5. Cassetta, L., and Pollard, J.W. (2023). A timeline of tumour-associated macrophage biology. Nat
730 Rev Cancer *23*, 238–257. https://doi.org/10.1038/s41568-022-00547-1.

731 6. Gooden, M.J.M., de Bock, G.H., Leffers, N., Daemen, T., and Nijman, H.W. (2011). The prognostic
732 influence of tumour-infiltrating lymphocytes in cancer: a systematic review with meta-analysis.
733 Br J Cancer *105*, 93–103. https://doi.org/10.1038/bjc.2011.189.

734 7. Brummel, K., Eerkens, A.L., De Bruyn, M., and Nijman, H.W. (2023). Tumour-infiltrating
735 lymphocytes: from prognosis to treatment selection. Br J Cancer *128*, 451–458.
736 https://doi.org/10.1038/s41416-022-02119-4.

737 8. Russell, S.J., Peng, K.-W., and Bell, J.C. (2012). Oncolytic virotherapy. Nat Biotechnol *30*, 658–670.
738 https://doi.org/10.1038/nbt.2287.

739 9. Bhatt, D.K., and Daemen, T. (2024). Molecular Circuits of Immune Sensing and Response to
740 Oncolytic Virotherapy. IJMS *25*, 4691. https://doi.org/10.3390/ijms25094691.

741 10. Denton, N., Chen, C.-Y., Scott, T., and Cripe, T. (2016). Tumor-Associated Macrophages in
742 Oncolytic Virotherapy: Friend or Foe? Biomedicines *4*, 13.
743 https://doi.org/10.3390/biomedicines4030013.

744 11. Jakeman, P.G., Hills, T.E., Fisher, K.D., and Seymour, L.W. (2015). Macrophages and their
745 interactions with oncolytic viruses. Current Opinion in Pharmacology *24*, 23–29.
746 https://doi.org/10.1016/j.coph.2015.06.007.

747 12. Mealiea, D., and McCart, J.A. (2022). Cutting both ways: the innate immune response to
748 oncolytic virotherapy. Cancer Gene Ther *29*, 629–646. https://doi.org/10.1038/s41417-021-
749 00351-3.

750 13. Hofman, L., Lawler, S.E., and Lamfers, M.L.M. (2021). The Multifaceted Role of Macrophages in
751 Oncolytic Virotherapy. Viruses *13*, 1570. https://doi.org/10.3390/v13081570.

752 14. DeNardo, D.G., and Ruffell, B. (2019). Macrophages as regulators of tumour immunity and
753 immunotherapy. Nat Rev Immunol *19*, 369–382. https://doi.org/10.1038/s41577-019-0127-6.

754 15. Bhatt, D.K., Wekema, L., Carvalho Barros, L.R., Chammas, R., and Daemen, T. (2021). A
755 systematic analysis on the clinical safety and efficacy of onco-virotherapy. Molecular Therapy -
756 Oncolytics *23*, 239–253. https://doi.org/10.1016/j.omto.2021.09.008.

757 16. Li, Z., Jiang, Z., Zhang, Y., Huang, X., and Liu, Q. (2020). Efficacy and Safety of Oncolytic Viruses in
758 Randomized Controlled Trials: A Systematic Review and Meta-Analysis. Cancers (Basel) *12*.
759 https://doi.org/10.3390/cancers12061416.

760 17. Bhatt, D.K., Chammas, R., and Daemen, T. (2021). Resistance Mechanisms Influencing Oncolytic
761 Virotherapy, a Systematic Analysis. Vaccines *9*, 1166. https://doi.org/10.3390/vaccines9101166.

762 18. de Gruijl, T.D., Janssen, A.B., and van Beusechem, V.W. (2015). Arming oncolytic viruses to
763 leverage antitumor immunity. Expert Opin Biol Ther *15*, 959–971.
764 https://doi.org/10.1517/14712598.2015.1044433.

765 19. Kaufman, H.L., Kohlhapp, F.J., and Zloza, A. (2015). Oncolytic viruses: a new class of
766 immunotherapy drugs. Nature Reviews Drug Discovery *14*, 642–662.
767 https://doi.org/10.1038/nrd4663.

768 20. Smerdou, C., and Liljeström, P. (1999). Two-helper RNA system for production of recombinant
769 Semliki forest virus particles. J Virol *73*, 1092–1098. https://doi.org/10.1128/JVI.73.2.1092-
770 1098.1999.

771 21. Kurena, B., Müller, E., Christopoulos, P.F., Johnsen, I.B., Stankovic, B., Øynebråten, I., Corthay, A.,
772 and Zajakina, A. (2017). Generation and Functional In Vitro Analysis of Semliki Forest Virus
773 Vectors Encoding TNF-α and IFN-γ. Front. Immunol. *8*, 1667.
774 https://doi.org/10.3389/fimmu.2017.01667.

775 22. Sánchez-Paulete, A.R., Teijeira, Á., Quetglas, J.I., Rodríguez-Ruiz, M.E., Sánchez-Arráez, Á.,
776 Labiano, S., Etxeberria, I., Azpilikueta, A., Bolaños, E., Ballesteros-Briones, M.C., et al. (2018).
777 Intratumoral Immunotherapy with XCL1 and sFlt3L Encoded in Recombinant Semliki Forest Virus-
778 Derived Vectors Fosters Dendritic Cell-Mediated T-cell Cross-Priming. Cancer Res. *78*, 6643–
779 6654. https://doi.org/10.1158/0008-5472.CAN-18-0933.

780 23. Bhatt, D.K., Meuleman, S.L., Hoogeboom, B.N., and Daemen, T. (2024). Oncolytic alphavirus
781 replicons mediated recruitment and activation of T cells. iScience *27*, 109253.
782 https://doi.org/10.1016/j.isci.2024.109253.

783 24. Draghiciu, O., Boerma, A., Hoogeboom, B.N., Nijman, H.W., and Daemen, T. (2015). A rationally
784 designed combined treatment with an alphavirus-based cancer vaccine, sunitinib and low-dose
785 tumor irradiation completely blocks tumor development. Oncoimmunology *4*, e1029699.
786 https://doi.org/10.1080/2162402X.2015.1029699.

787 25. Ip, P.P., Boerma, A., Regts, J., Meijerhof, T., Wilschut, J., Nijman, H.W., and Daemen, T. (2014).
788 Alphavirus-based vaccines encoding nonstructural proteins of hepatitis C virus induce robust and
789 protective T-cell responses. Mol Ther *22*, 881–890. https://doi.org/10.1038/mt.2013.287.

790 26. Knudsen, M.L., Ljungberg, K., Tatoud, R., Weber, J., Esteban, M., and Liljeström, P. (2015).
791 Alphavirus replicon DNA expressing HIV antigens is an excellent prime for boosting with
792 recombinant modified vaccinia Ankara (MVA) or with HIV gp140 protein antigen. PLoS ONE *10*,
793 e0117042. https://doi.org/10.1371/journal.pone.0117042.

794 27. Öhlund, P., García-Arriaza, J., Zusinaite, E., Szurgot, I., Männik, A., Kraus, A., Ustav, M., Merits, A.,
795 Esteban, M., Liljeström, P., et al. (2018). DNA-launched RNA replicon vaccines induce potent anti-
796 Ebolavirus immune responses that can be further improved by a recombinant MVA boost. Sci
797 Rep *8*, 12459. https://doi.org/10.1038/s41598-018-31003-6.

798 28. Quetglas, J.I., Labiano, S., Aznar, M.Á., Bolaños, E., Azpilikueta, A., Rodriguez, I., Casales, E.,
799 Sánchez-Paulete, A.R., Segura, V., Smerdou, C., et al. (2015). Virotherapy with a Semliki Forest
800 Virus–Based Vector Encoding IL12 Synergizes with PD-1/PD-L1 Blockade. Cancer Immunology
801 Research *3*, 449–454. https://doi.org/10.1158/2326-6066.CIR-14-0216.

802 29. Ballesteros-Briones, M.C., Martisova, E., Casales, E., Silva-Pilipich, N., Buñuales, M., Galindo, J.,
803 Mancheño, U., Gorraiz, M., Lasarte, J.J., Kochan, G., et al. (2019). Short-Term Local Expression of
804 a PD-L1 Blocking Antibody from a Self-Replicating RNA Vector Induces Potent Antitumor
805 Responses. Mol Ther *27*, 1892–1905. https://doi.org/10.1016/j.ymthe.2019.09.016.

806 30. Komdeur, F.L., Singh, A., van de Wall, S., Meulenberg, J.J.M., Boerma, A., Hoogeboom, B.N.,
807 Paijens, S.T., Oyarce, C., de Bruyn, M., Schuuring, E., et al. (2021). First-in-Human Phase I Clinical
808 Trial of an SFV-Based RNA Replicon Cancer Vaccine against HPV-Induced Cancers. Mol Ther *29*,
809 611–625. https://doi.org/10.1016/j.ymthe.2020.11.002.

810 31. Eerkens, A.L., Esajas, M.D., Brummel, K., Vledder, A., Van Rooij, N., Plat, A., Avalos Haro, S.B.,
811 Paijens, S.T., Slagter-Menkema, L., Schuuring, E., et al. (2025). Vvax001, a Therapeutic Vaccine
812 for Patients with HPV16-positive High-grade Cervical Intraepithelial Neoplasia: a Phase II Trial.
813 Clinical Cancer Research. https://doi.org/10.1158/1078-0432.CCR-24-1662.

814 32. Chen, S. (2023). Manipulating immune cells — a therapeutic strategy for cancer and
815 inflammatory disease: https://doi.org/10.33612/diss.822658140.

816 33. Bhatt, D.K., Janzen, T., Daemen, T., and Weissing, F.J. (2022). Modelling the spatial dynamics of
817 oncolytic virotherapy in the presence of virus-resistant tumour cells. PLoS Comput Biol *18*,
818 e1010076. https://doi.org/10.1371/journal.pcbi.1010076.

819 34. Bhatt, D.K., Janzen, T., Daemen, T., and Weissing, F.J. (2024). Effects of virus-induced
820 immunogenic cues on oncolytic virotherapy. Sci Rep *14*, 28861. https://doi.org/10.1038/s41598-
821 024-80542-8.

822 35. Altan-Bonnet, G., and Mukherjee, R. (2019). Cytokine-mediated communication: a quantitative
823 appraisal of immune complexity. Nat Rev Immunol *19*, 205–217.
824 https://doi.org/10.1038/s41577-019-0131-x.

825 36. Eddy, J.A., Thorsson, V., Lamb, A.E., Gibbs, D.L., Heimann, C., Yu, J.X., Chung, V., Chae, Y., Dang,
826 K., Vincent, B.G., et al. (2020). CRI iAtlas: an interactive portal for immuno-oncology research.
827 F1000Res *9*, 1028. https://doi.org/10.12688/f1000research.25141.1.

828 37. Kurena, B., Müller, E., Christopoulos, P.F., Johnsen, I.B., Stankovic, B., Øynebråten, I., Corthay, A.,
829 and Zajakina, A. (2017). Generation and Functional In Vitro Analysis of Semliki Forest Virus
830 Vectors Encoding TNF-α and IFN-γ. Frontiers in Immunology *8*.
831 https://doi.org/10.3389/fimmu.2017.01667.

832 38. Weigelin, B., den Boer, A.Th., Wagena, E., Broen, K., Dolstra, H., de Boer, R.J., Figdor, C.G.,
833 Textor, J., and Friedl, P. (2021). Cytotoxic T cells are able to efficiently eliminate cancer cells by
834 additive cytotoxicity. Nat Commun *12*, 5217. https://doi.org/10.1038/s41467-021-25282-3.

835 39. Masemann, D., Köther, K., Kuhlencord, M., Varga, G., Roth, J., Lichty, B.D., Rapp, U.R., Wixler, V.,
836 and Ludwig, S. (2018). Oncolytic influenza virus infection restores immunocompetence of lung
837 tumor-associated alveolar macrophages. OncoImmunology *7*, e1423171.
838 https://doi.org/10.1080/2162402X.2017.1423171.

839 40. Pulaski, B.A., Smyth, M.J., and Ostrand-Rosenberg, S. (2002). Interferon-gamma-dependent
840 phagocytic cells are a critical component of innate immunity against metastatic mammary
841 carcinoma. Cancer Res *62*, 4406–4412.

842 41. Van Den Bossche, W.B.L., Kleijn, A., Teunissen, C.E., Voerman, J.S.A., Teodosio, C., Noske, D.P.,
843 Van Dongen, J.J.M., Dirven, C.M.F., and Lamfers, M.L.M. (2018). Oncolytic virotherapy in
844 glioblastoma patients induces a tumor macrophage phenotypic shift leading to an altered
845 glioblastoma microenvironment. Neuro-Oncology *20*, 1494–1504.
846 https://doi.org/10.1093/neuonc/noy082.

847 42. Meisen, W.H., Wohleb, E.S., Jaime-Ramirez, A.C., Bolyard, C., Yoo, J.Y., Russell, L., Hardcastle, J.,
848 Dubin, S., Muili, K., Yu, J., et al. (2015). The Impact of Macrophage- and Microglia-Secreted TNFα
849 on Oncolytic HSV-1 Therapy in the Glioblastoma Tumor Microenvironment. Clin Cancer Res *21*,
850 3274–3285. https://doi.org/10.1158/1078-0432.CCR-14-3118.

851 43. Saha, D., Martuza, R.L., and Rabkin, S.D. (2017). Macrophage Polarization Contributes to
852 Glioblastoma Eradication by Combination Immunovirotherapy and Immune Checkpoint
853 Blockade. Cancer Cell *32*, 253-267.e5. https://doi.org/10.1016/j.ccell.2017.07.006.

854 44. Fulci, G., Dmitrieva, N., Gianni, D., Fontana, E.J., Pan, X., Lu, Y., Kaufman, C.S., Kaur, B., Lawler,
855 S.E., Lee, R.J., et al. (2007). Depletion of Peripheral Macrophages and Brain Microglia Increases
856 Brain Tumor Titers of Oncolytic Viruses. Cancer Research *67*, 9398–9406.
857 https://doi.org/10.1158/0008-5472.CAN-07-1063.

858 45. Thoresen, D., Wang, W., Galls, D., Guo, R., Xu, L., and Pyle, A.M. (2021). The molecular
859 mechanism of RIG-I activation and signaling. Immunol Rev *304*, 154–168.
860 https://doi.org/10.1111/imr.13022.

861 46. Rojas, J.J., Sampath, P., Bonilla, B., Ashley, A., Hou, W., Byrd, D., and Thorne, S.H. (2016).
862 Manipulating TLR Signaling Increases the Anti-tumor T Cell Response Induced by Viral Cancer
863 Therapies. Cell Rep *15*, 264–273. https://doi.org/10.1016/j.celrep.2016.03.017.

864 47. Muñoz-Rojas, A.R., Kelsey, I., Pappalardo, J.L., Chen, M., and Miller-Jensen, K. (2021). Co-
865 stimulation with opposing macrophage polarization cues leads to orthogonal secretion programs
866 in individual cells. Nat Commun *12*, 301. https://doi.org/10.1038/s41467-020-20540-2.

867 48. Piccolo, V., Curina, A., Genua, M., Ghisletti, S., Simonatto, M., Sabò, A., Amati, B., Ostuni, R., and
868 Natoli, G. (2017). Opposing macrophage polarization programs show extensive epigenomic and
869 transcriptional cross-talk. Nat Immunol *18*, 530–540. https://doi.org/10.1038/ni.3710.

870 49. Stout, R.D., Jiang, C., Matta, B., Tietzel, I., Watkins, S.K., and Suttles, J. (2005). Macrophages
871 Sequentially Change Their Functional Phenotype in Response to Changes in Microenvironmental
872 Influences. The Journal of Immunology *175*, 342–349.
873 https://doi.org/10.4049/jimmunol.175.1.342.

874 50. Lavin, Y., Winter, D., Blecher-Gonen, R., David, E., Keren-Shaul, H., Merad, M., Jung, S., and Amit,
875 I. (2014). Tissue-Resident Macrophage Enhancer Landscapes Are Shaped by the Local
876 Microenvironment. Cell *159*, 1312–1326. https://doi.org/10.1016/j.cell.2014.11.018.

877 51. Trofimova, O., Korotkaja, K., Skrastina, D., Jansons, J., Spunde, K., Isaguliants, M., and Zajakina, A.
878 (2021). Alphavirus-Driven Interferon Gamma (IFNg) Expression Inhibits Tumor Growth in
879 Orthotopic 4T1 Breast Cancer Model. Vaccines (Basel) *9*, 1247.
880 https://doi.org/10.3390/vaccines9111247.

881 52. Müller, E., Speth, M., Christopoulos, P.F., Lunde, A., Avdagic, A., Øynebråten, I., and Corthay, A.
882 (2018). Both Type I and Type II Interferons Can Activate Antitumor M1 Macrophages When
883 Combined With TLR Stimulation. Front. Immunol. *9*, 2520.
884 https://doi.org/10.3389/fimmu.2018.02520.

885 53. Meissner, R., Wixler, V., Wulfert, F.P., Jacob, J.C., Hale, B.G., Robeck, T., Masemann, D.,
886 Boergeling, Y., and Ludwig, S. (2023). Replication-incompetent influenza A viruses armed with
887 IFN-γ effectively mediate immune modulation and tumor destruction in mice harboring lung
888 cancer. Molecular Therapy - Oncolytics *31*, 100741.
889 https://doi.org/10.1016/j.omto.2023.100741.

890 54. Bourgeois-Daigneault, M.-C., Roy, D.G., Falls, T., Twumasi-Boateng, K., St-Germain, L.E.,
891 Marguerie, M., Garcia, V., Selman, M., Jennings, V.A., Pettigrew, J., et al. (2016). Oncolytic
892 vesicular stomatitis virus expressing interferon-σ has enhanced therapeutic activity. Molecular
893 Therapy - Oncolytics *3*, 16001. https://doi.org/10.1038/mto.2016.1.

894 55. Singh, A., Koutsoumpli, G., Van De Wall, S., and Daemen, T. (2019). An alphavirus-based
895 therapeutic cancer vaccine: from design to clinical trial. Cancer Immunol Immunother *68*, 849–
896 859. https://doi.org/10.1007/s00262-018-2276-z.

897 56. Groeneveldt, C., Kinderman, P., Van Den Wollenberg, D.J.M., Van Den Oever, R.L., Middelburg, J.,
898 Mustafa, D.A.M., Hoeben, R.C., Van Der Burg, S.H., Van Hall, T., and Van Montfoort, N. (2020).
899 Preconditioning of the tumor microenvironment with oncolytic reovirus converts CD3-bispecific
900 antibody treatment into effective immunotherapy. J Immunother Cancer *8*, e001191.
901 https://doi.org/10.1136/jitc-2020-001191.

902 57. Groeneveldt, C., van Ginkel, J.Q., Kinderman, P., Sluijter, M., Griffioen, L., Labrie, C., van den
903 Wollenberg, D.J.M., Hoeben, R.C., van der Burg, S.H., ten Dijke, P., et al. (2023). Intertumoral
904 Differences Dictate the Outcome of TGF-β Blockade on the Efficacy of Viro-Immunotherapy.
905 Cancer Research Communications *3*, 325–337. https://doi.org/10.1158/2767-9764.CRC-23-0019.

906 58. Groeneveldt, C., Kinderman, P., Griffioen, L., Rensing, O., Labrie, C., van den Wollenberg, D.J.M.,
907 Hoeben, R.C., Coffey, M., Loghmani, H., Verdegaal, E.M.E., et al. (2024). Neutralizing Antibodies
908 Impair the Oncolytic Efficacy of Reovirus but Permit Effective Combination with T cell–Based
909 Immunotherapies. Cancer Immunology Research *12*, 334–349. https://doi.org/10.1158/2326-
910 6066.CIR-23-0480.

911

Figure 1

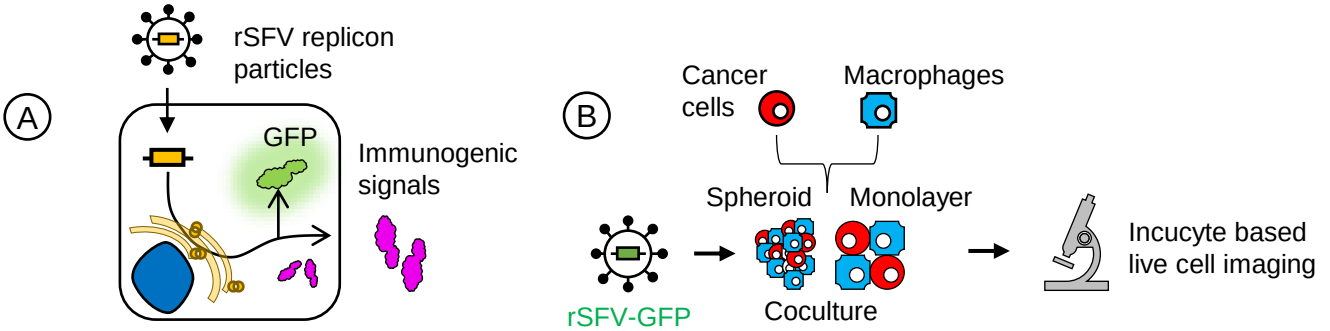
A
rSFV replicon particles
GFP
Immunogenic signals
B
Cancer cells
Macrophages
Spheroid
Monolayer
rSFV-GFP
Coculture
Incucyte based live cell imaging

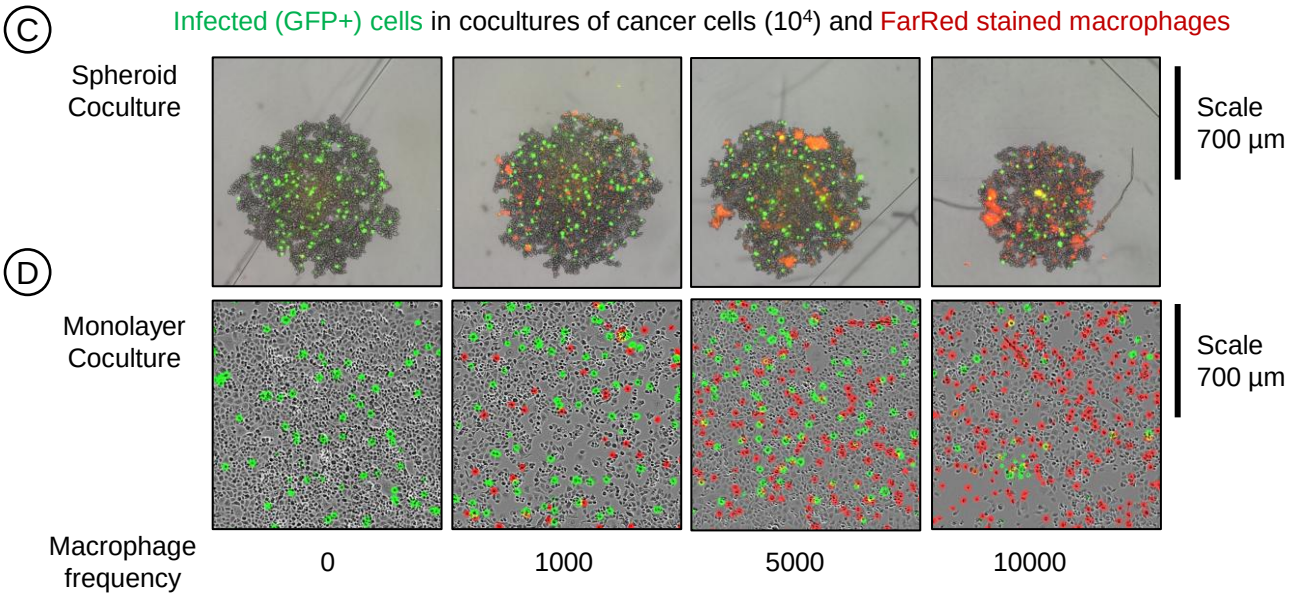
C
Infected (GFP+) cells in cocultures of cancer cells (10^4) and FarRed stained macrophages
Spheroid Coculture
Scale 700 µm
D
Monolayer Coculture
Scale 700 µm
Macrophage frequency
0
1000
5000
10000

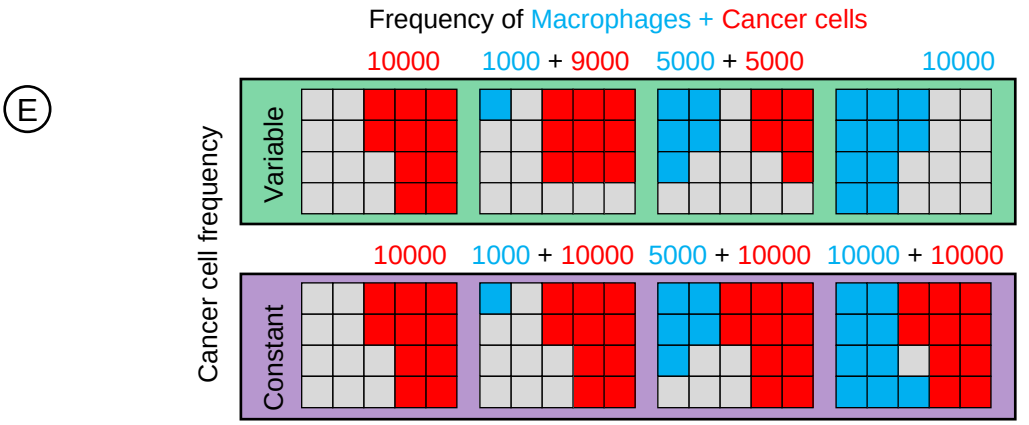
E
Frequency of Macrophages + Cancer cells
10000
1000 + 9000
5000 + 5000
10000
Variable
10000
1000 + 10000
5000 + 10000
10000 + 10000
Constant
Cancer cell frequency

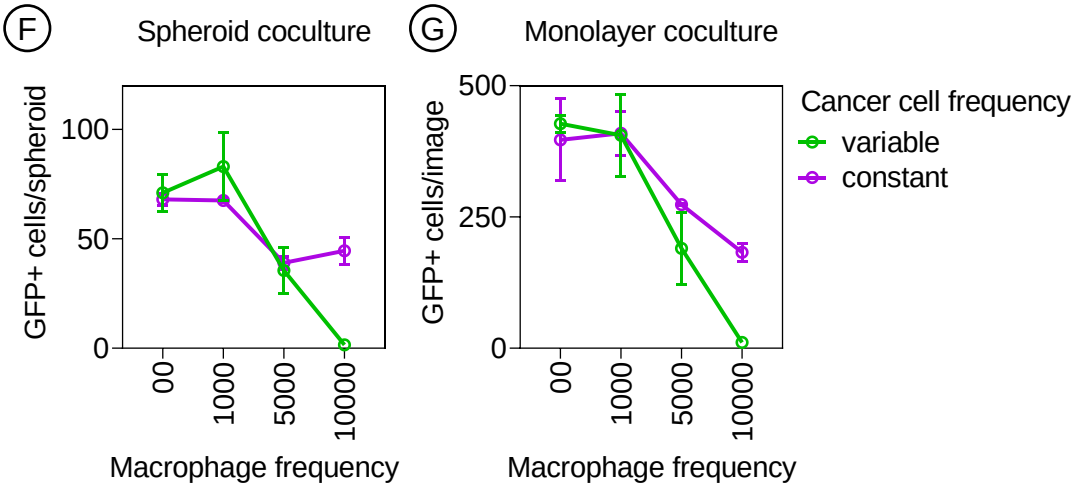
F
Spheroid coculture
GFP+ cells/spheroid
100
50
0
00
1000
5000
10000
Macrophage frequency
G
Monolayer coculture
GFP+ cells/image
500
250
0
00
1000
5000
10000
Macrophage frequency
Cancer cell frequency
variable
constant

Figure 2

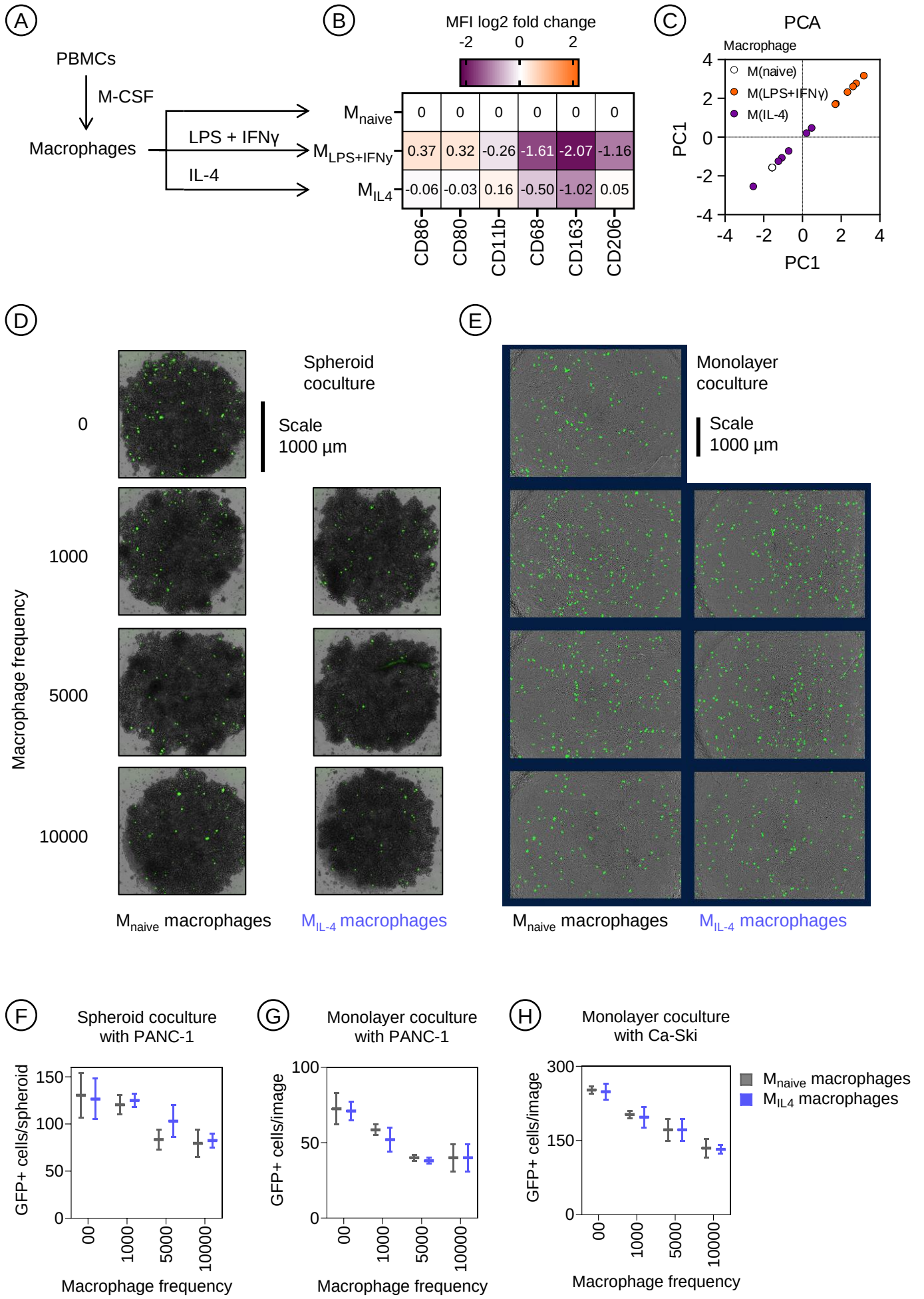
A
PBMCs
M-CSF
Macrophages
LPS + IFNγ
IL-4
B
MFI log2 fold change
-2
0
2
M naive
M LPS+IFNγ
M IL4
0 0 0 0 0 0
0.37 0.32 -0.26 -1.61 -2.07 -1.16
-0.06 -0.03 0.16 -0.50 -1.02 0.05
CD86
CD80
CD11b
CD68
CD163
CD206
C
PCA
Macrophage
M(naive)
M(LPS+IFNγ)
M(IL-4)
PC1
PC1
D
Spheroid coculture
Scale 1000 µm
Macrophage frequency
0
1000
5000
10000
M naive macrophages
M IL-4 macrophages
E
Monolayer coculture
Scale 1000 µm
M naive macrophages
M IL-4 macrophages
F
Spheroid coculture with PANC-1
GFP+ cells/spheroid
Macrophage frequency
G
Monolayer coculture with PANC-1
GFP+ cells/image
Macrophage frequency
H
Monolayer coculture with Ca-Ski
GFP+ cells/image
Macrophage frequency
M naive macrophages
M IL4 macrophages

Figure 3

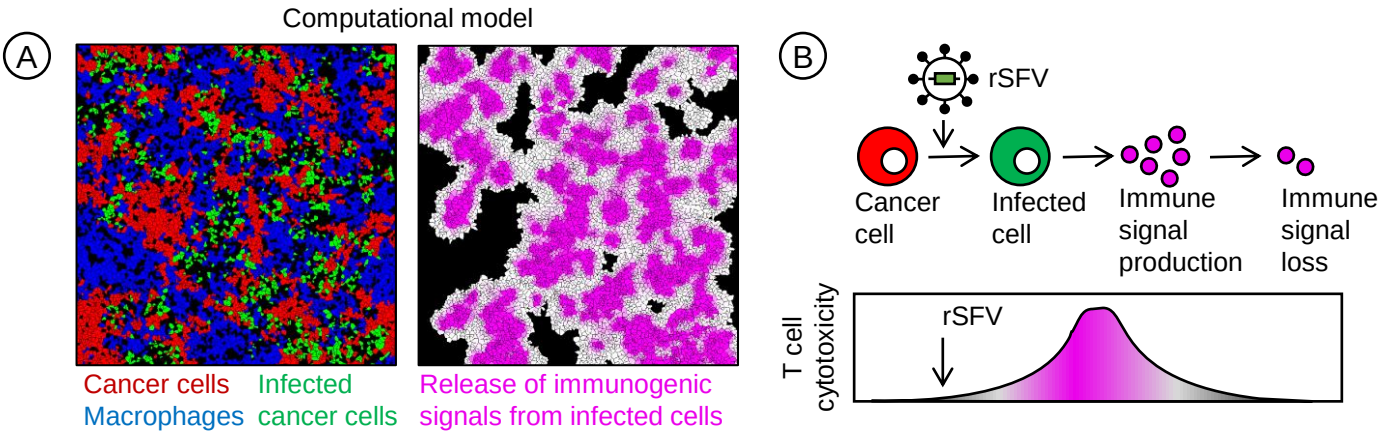
A
Computational model
Cancer cells
Macrophages
Infected cancer cells
Release of immunogenic signals from infected cells
B
rSFV
Cancer cell
Infected cell
Immune signal production
Immune signal loss
T cell cytotoxicity
rSFV

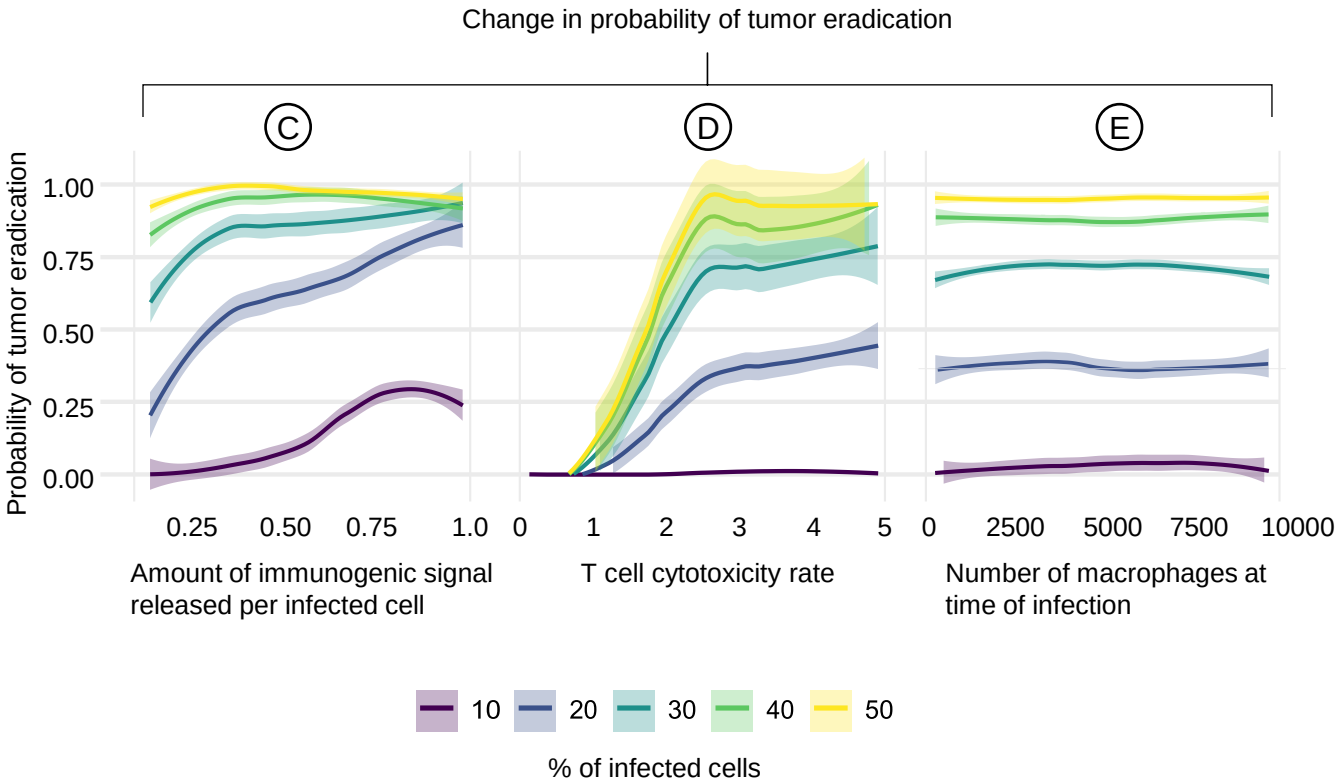
Change in probability of tumor eradication
C
D
E
Probability of tumor eradication
1.00
0.75
0.50
0.25
0.00
0.25
0.50
0.75
1.0
0
1
2
3
4
5
0
2500
5000
7500
10000
Amount of immunogenic signal released per infected cell
T cell cytotoxicity rate
Number of macrophages at time of infection
10
20
30
40
50
% of infected cells

Figure 4

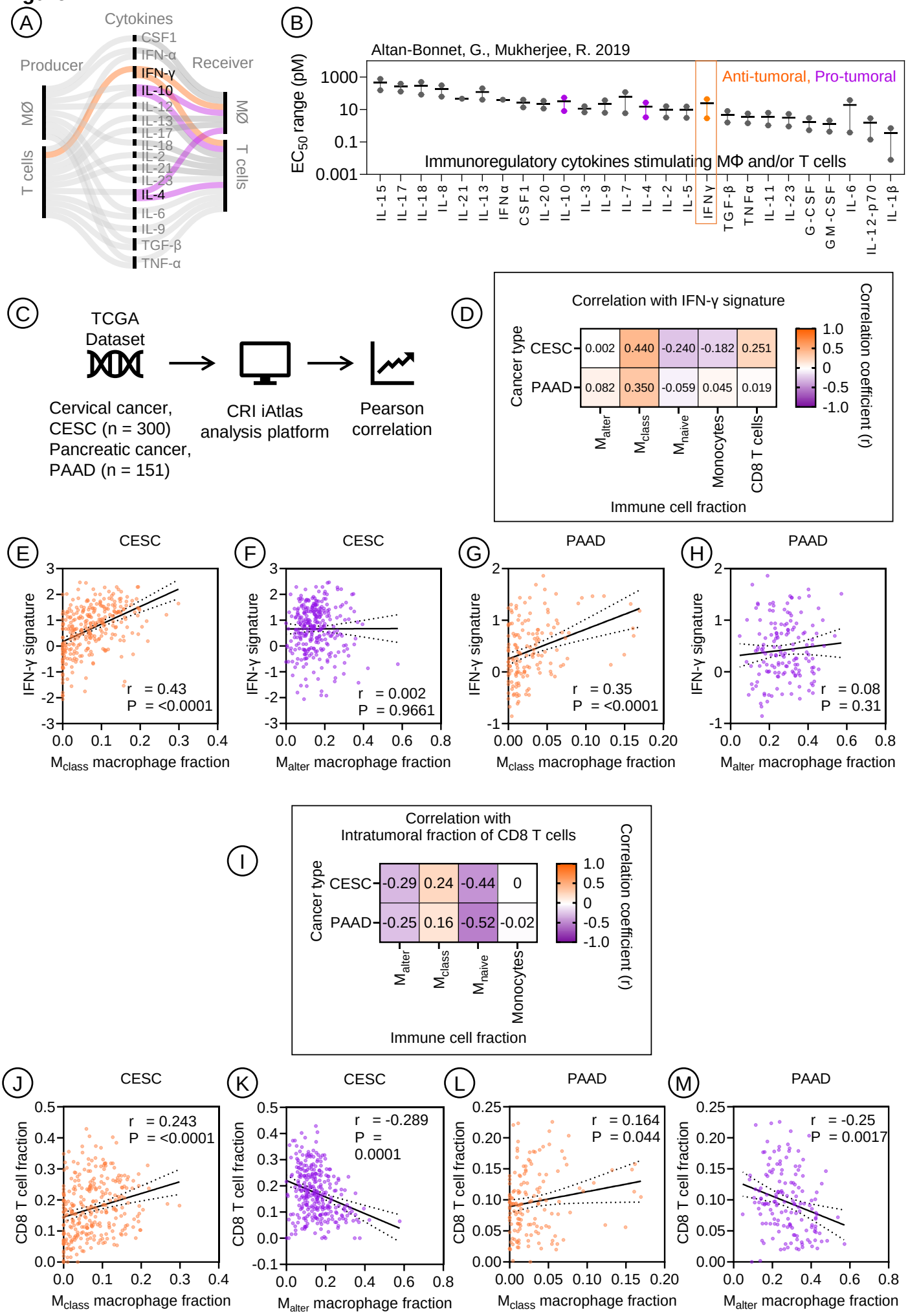
A
Cytokines
Producer
Receiver
MØ
T cells
CSF1
IFN-α
IFN-γ
IL-10
IL-12
IL-13
IL-17
IL-18
IL-2
IL-21
IL-23
IL-4
IL-6
IL-9
TGF-β
TNF-α
B
Altan-Bonnet, G., Mukherjee, R. 2019
EC50 range (pM)
Anti-tumoral, Pro-tumoral
Immunoregulatory cytokines stimulating MΦ and/or T cells
C
TCGA Dataset
Cervical cancer, CESC (n = 300)
Pancreatic cancer, PAAD (n = 151)
CRI iAtlas analysis platform
Pearson correlation
D
Correlation with IFN-γ signature
Cancer type
CESC 0.002 0.440 -0.240 -0.182 0.251
PAAD 0.082 0.350 -0.059 0.045 0.019
Malter Mclass Mnaive Monocytes CD8 T cells
Immune cell fraction
Correlation coefficient (r)
E CESC r = 0.43 P = <0.0001
F CESC r = 0.002 P = 0.9661
G PAAD r = 0.35 P = <0.0001
H PAAD r = 0.08 P = 0.31
IFN-γ signature
Mclass macrophage fraction
Malter macrophage fraction
I
Correlation with Intratumoral fraction of CD8 T cells
Cancer type
CESC -0.29 0.24 -0.44 0
PAAD -0.25 0.16 -0.52 -0.02
Malter Mclass Mnaive Monocytes
Immune cell fraction
Correlation coefficient (r)
J CESC r = 0.243 P = <0.0001
K CESC r = -0.289 P = 0.0001
L PAAD r = 0.164 P = 0.044
M PAAD r = -0.25 P = 0.0017
CD8 T cell fraction
Mclass macrophage fraction
Malter macrophage fraction

Figure 5

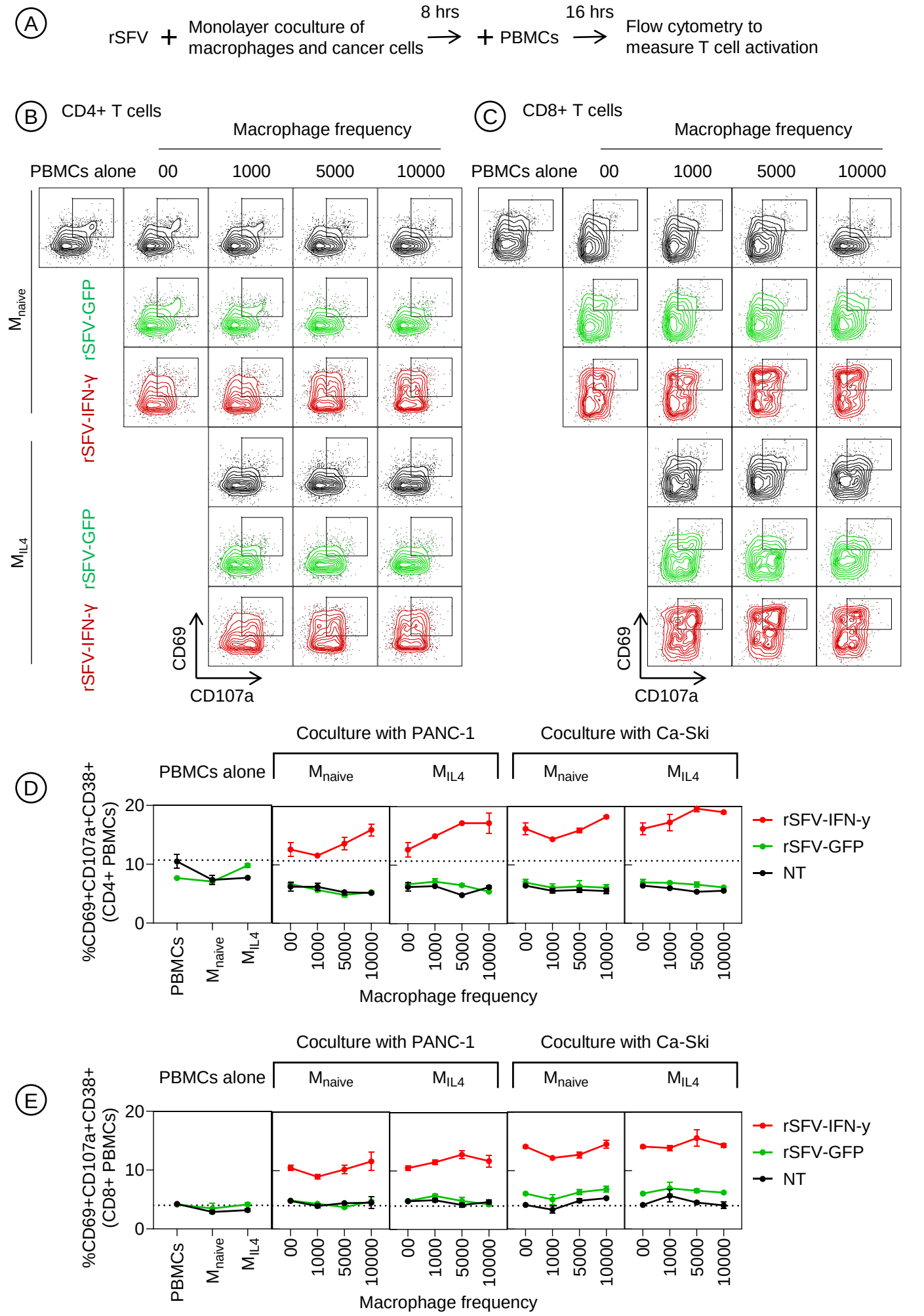
A
rSFV + Monolayer coculture of macrophages and cancer cells
8 hrs
+ PBMCs
16 hrs
Flow cytometry to measure T cell activation
B
CD4+ T cells
Macrophage frequency
PBMCs alone
00
1000
5000
10000
M naive
M IL4
rSFV-GFP
rSFV-IFN-γ
CD69
CD107a
C
CD8+ T cells
Macrophage frequency
PBMCs alone
00
1000
5000
10000
CD69
CD107a
D
Coculture with PANC-1
Coculture with Ca-Ski
PBMCs alone
M naive
M IL4
%CD69+CD107a+CD38+ (CD4+ PBMCs)
20
10
0
PBMCs
00
1000
5000
10000
Macrophage frequency
rSFV-IFN-y
rSFV-GFP
NT
E
Coculture with PANC-1
Coculture with Ca-Ski
PBMCs alone
M naive
M IL4
%CD69+CD107a+CD38+ (CD8+ PBMCs)
20
10
0
PBMCs
00
1000
5000
10000
Macrophage frequency
rSFV-IFN-y
rSFV-GFP
NT

Figure 6

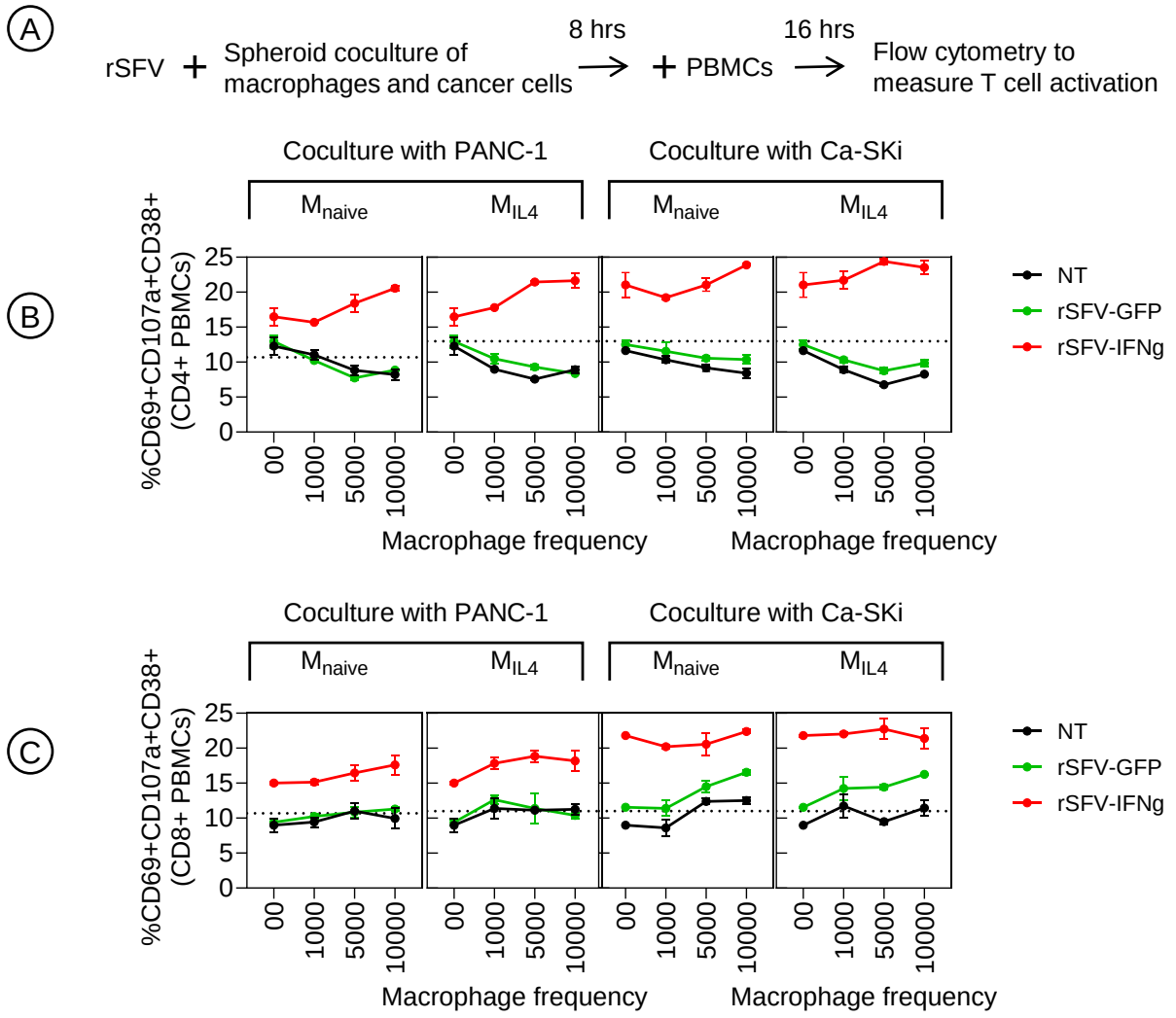
A
rSFV + Spheroid coculture of macrophages and cancer cells
8 hrs
+ PBMCs
16 hrs
Flow cytometry to measure T cell activation
B
Coculture with PANC-1
Coculture with Ca-SKi
M naive
M IL4
%CD69+CD107a+CD38+ (CD4+ PBMCs)
25
20
15
10
5
0
00
1000
5000
10000
Macrophage frequency
NT
rSFV-GFP
rSFV-IFNg
C
Coculture with PANC-1
Coculture with Ca-SKi
M naive
M IL4
%CD69+CD107a+CD38+ (CD8+ PBMCs)
25
20
15
10
5
0
00
1000
5000
10000
Macrophage frequency
NT
rSFV-GFP
rSFV-IFNg

Figure 7

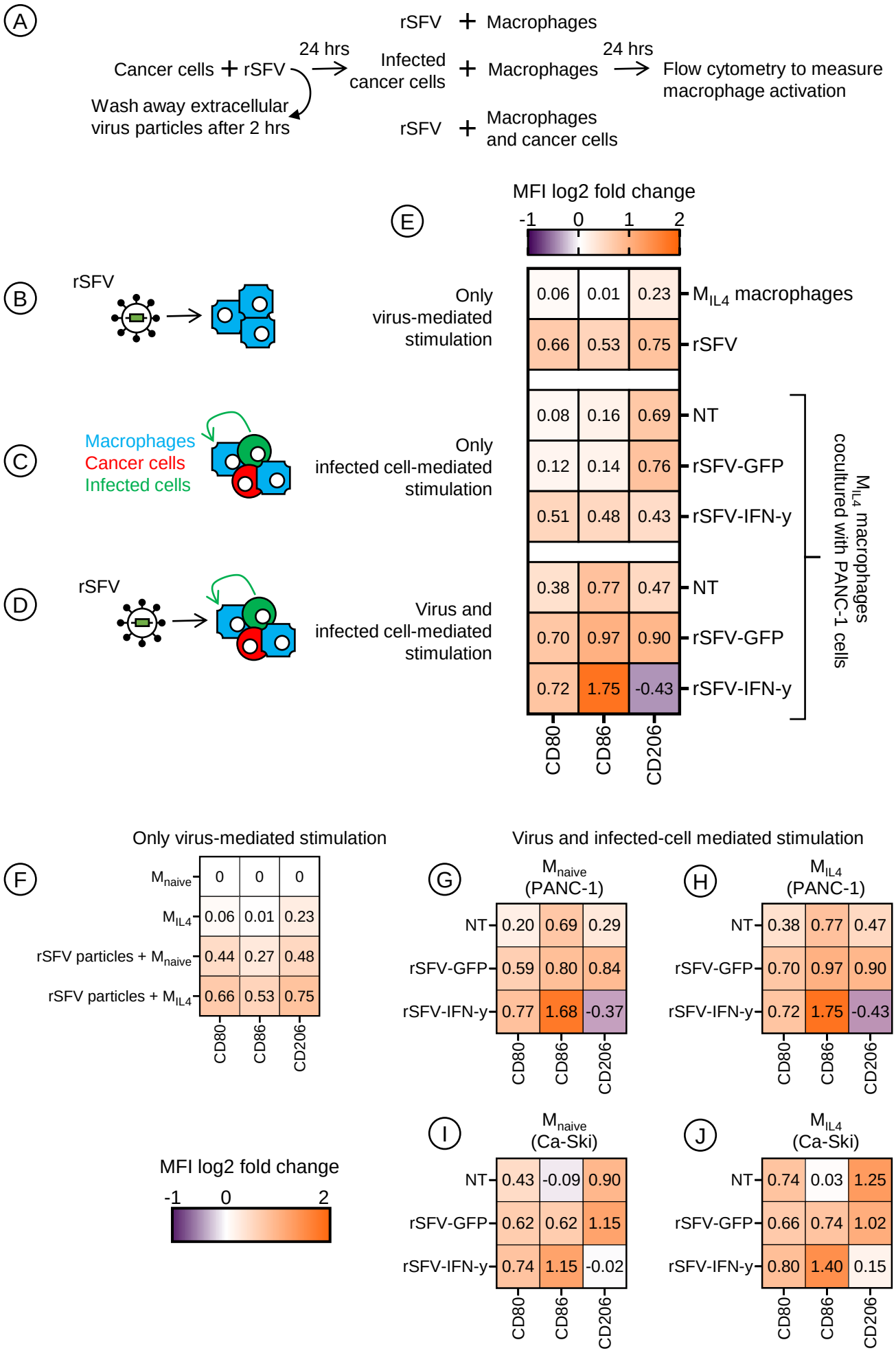
A
Cancer cells + rSFV
24 hrs
Wash away extracellular virus particles after 2 hrs
rSFV + Macrophages
Infected cancer cells + Macrophages
24 hrs
Flow cytometry to measure macrophage activation
rSFV + Macrophages and cancer cells
B
rSFV
C
Macrophages
Cancer cells
Infected cells
D
rSFV
E
MFI log2 fold change
-1 0 1 2
Only virus-mediated stimulation
Only infected cell-mediated stimulation
Virus and infected cell-mediated stimulation
0.06 0.01 0.23 M_IL4 macrophages
0.66 0.53 0.75 rSFV
0.08 0.16 0.69 NT
0.12 0.14 0.76 rSFV-GFP
0.51 0.48 0.43 rSFV-IFN-y
0.38 0.77 0.47 NT
0.70 0.97 0.90 rSFV-GFP
0.72 1.75 -0.43 rSFV-IFN-y
M_IL4 macrophages cocultured with PANC-1 cells
CD80 CD86 CD206
F
Only virus-mediated stimulation
M_naive 0 0 0
M_IL4 0.06 0.01 0.23
rSFV particles + M_naive 0.44 0.27 0.48
rSFV particles + M_IL4 0.66 0.53 0.75
CD80 CD86 CD206
Virus and infected-cell mediated stimulation
G
M_naive (PANC-1)
NT 0.20 0.69 0.29
rSFV-GFP 0.59 0.80 0.84
rSFV-IFN-y 0.77 1.68 -0.37
H
M_IL4 (PANC-1)
NT 0.38 0.77 0.47
rSFV-GFP 0.70 0.97 0.90
rSFV-IFN-y 0.72 1.75 -0.43
I
M_naive (Ca-Ski)
NT 0.43 -0.09 0.90
rSFV-GFP 0.62 0.62 1.15
rSFV-IFN-y 0.74 1.15 -0.02
J
M_IL4 (Ca-Ski)
NT 0.74 0.03 1.25
rSFV-GFP 0.66 0.74 1.02
rSFV-IFN-y 0.80 1.40 0.15
MFI log2 fold change
-1 0 2

Figure 8

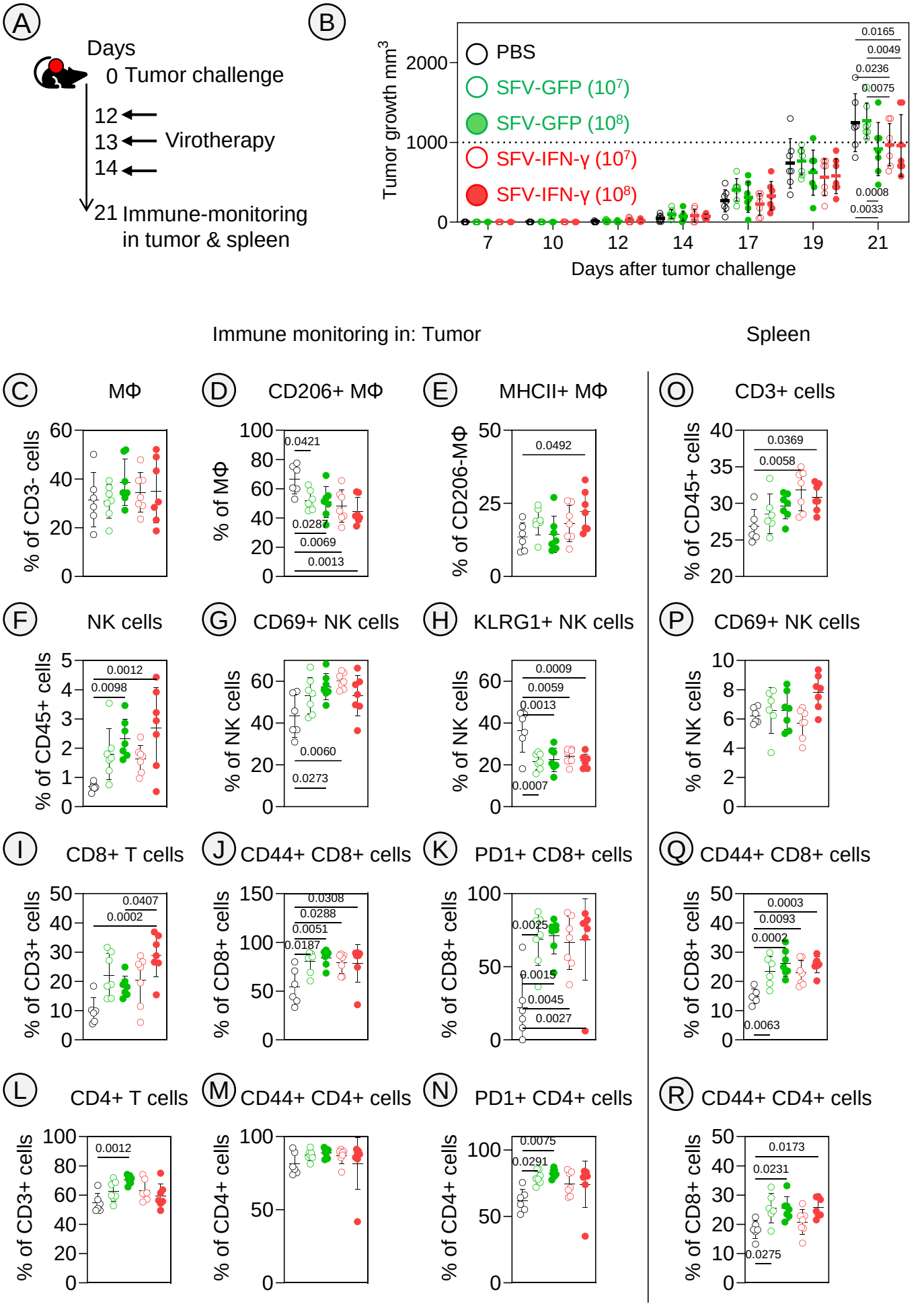
A
Days
0 Tumor challenge
12
13 Virotherapy
14
21 Immune-monitoring in tumor & spleen
B
PBS
SFV-GFP (10^7)
SFV-GFP (10^8)
SFV-IFN-γ (10^7)
SFV-IFN-γ (10^8)
Tumor growth mm^3
Days after tumor challenge
0.0165
0.0049
0.0236
0.0075
0.0008
0.0033
Immune monitoring in: Tumor
Spleen
C MΦ
% of CD3- cells
D CD206+ MΦ
% of MΦ
0.0421
0.0287
0.0069
0.0013
E MHCII+ MΦ
% of CD206-MΦ
0.0492
O CD3+ cells
% of CD45+ cells
0.0369
0.0058
F NK cells
% of CD45+ cells
0.0012
0.0098
G CD69+ NK cells
% of NK cells
0.0060
0.0273
H KLRG1+ NK cells
% of NK cells
0.0009
0.0059
0.0013
0.0007
P CD69+ NK cells
% of NK cells
I CD8+ T cells
% of CD3+ cells
0.0407
0.0002
J CD44+ CD8+ cells
% of CD8+ cells
0.0308
0.0288
0.0051
0.0187
K PD1+ CD8+ cells
% of CD8+ cells
0.0025
0.0015
0.0045
0.0027
Q CD44+ CD8+ cells
% of CD8+ cells
0.0003
0.0093
0.0002
0.0063
L CD4+ T cells
% of CD3+ cells
0.0012
M CD44+ CD4+ cells
% of CD4+ cells
N PD1+ CD4+ cells
% of CD4+ cells
0.0075
0.0291
R CD44+ CD4+ cells
% of CD8+ cells
0.0173
0.0231
0.0275